Available online at www.sciencedirect.com
SCIENCE DIRECT®
International Journal of Mass Spectrometry 227 (2003) 525–554
International Journal of Mass Spectrometry
www.elsevier.com/locate/ijms

The proton affinity scale, and effects of ion structure and solvation

Michael Meot-Ner (Mautner)[a,b,*]

[a] *Department of Chemistry, University of Canterbury, Christchurch 8001, New Zealand*
[b] *Department of Chemistry, Virginia Commonwealth University, Richmond, VA 23284, USA*

Received 6 April 2002; accepted 21 August 2002

Abstract

In the last three decades, several extensive thermochemical ladders were constructed that connect molecules over a wide range of gas-phase basicities (GBs, i.e., $-\Delta G^\circ$ protonation) and proton affinities (PAs, i.e., $-\Delta H^\circ$ protonation). The data include GB ladders from low pressure ion cyclotron resonance (ICR), GB and PA ladders from pulsed high pressure mass spectrometry (PHPMS), absolute reference PAs from spectroscopic measurements, and ab initio calculations. Comparison amongst the ladders identifies some systematic expansions or contractions (mostly <10%), mainly due to uncertainties in temperature measurement. After global adjustments for these effects and anchoring to accurate local standards, all the data are consistent, including the directly measured PA ladders from variable temperature PHPMS measurements. Bracketing experiments and association thermochemistry provide further independent verification of the GB and PA scales. The derived entropies of protonation (S_p) from PHPMS measurements and theoretical calculations are structurally reasonable and mutually consistent, which supports the entropy results and the consistencies of the GB and PA scales. Special structural effects such as internal hydrogen bonds in polyfunctional and biomolecules ions can also be quantified. The overall data suggest that the GB and PA scales, spanning a range of 120 kcal mol^{-1} for 38 reference compounds, have been established within ±0.8 kcal mol^{-1}, and the S_p values within ±1.5 cal mol^{-1} K^{-1}, which may be the limits of accuracy of current methods. The gas-phase data, used in thermochemical cycles, allows calculating the solvation energies of ions. Molecular and solvation effects can be separated, and the latter decomposed into continuum and hydrogen bonding terms. Altogether, the gas-phase data allows decomposing the energetics of organic acid–base chemistry into structurally sensible and quantitatively understandable factors.

Keywords: Basicity; Energetics; Hydrogen bonds; Ion solvation; Proton affinity; Thermochemistry

1. Introduction: definitions and an overview

Protonated species are central to many chemical processes, such as acid–base phenomena, astrochemistry, radiation chemistry, chemical ionization mass spectrometry, catalysis, crystal structure, surface chemistry, industrial catalysis, and many aspects of biophysics such as protein conformation, enzyme catalysis and membrane transport. The location of the proton in these environments depends both on the binding energies of the proton to bases and on the strong interactions of the protonated species with

* Tel.: +64-3-364-2110; fax: +64-3-364-2110.
E-mail address: m.mautner@chem.canterbury.ac.nz (M. Meot-Ner (Mautner)).

1387-3806/03/$ – see front matter © 2003 Elsevier Science B.V. All rights reserved.
doi:10.1016/S1387-3806(03)00100-3

the surrounding medium. With the advent of mass spectrometry it became possible to determine the intrinsic gas-phase basicities, as well as the acidities, of individual molecules and to separate molecular and solvation effects. These developments constitute a major advance in fundamental acid–base chemistry.

The results of over three decades of work by numerous researchers were integrated in an evaluated NIST tabulation of data on over 2000 compounds which may be considered the current benchmark [1], also referred below as Hun/Lia. The GB and PA values for key standards were based mainly on recent PHPMS scales of Meot-Ner (Mautner) and Sieck [2], also referred below as Mau/Sie, and of Szulejko and McMahon [3] also referred below as Szu/McM, and on ab initio G2 calculations of Radom and coworkers [4,5] also referred below as Eas/Rad. The results were checked for consistency with previous ICR [6] and PHPMS [7,8] ladders. This review will summarize the method used in the NIST tabulations [1] and will show that, with small global adjustments and re-anchoring, the directly measured PA scales [2,3] further support the tabulated PA values.

The gas-phase basicity ($GB = -\Delta G_1^\circ$) and proton affinity ($PA = -\Delta H_1^\circ$) are defined by the thermochemistry of reaction (1). The difference is of course $T\Delta S_1^\circ$, and in addition to this term, a useful term is the protonation entropy $S_p^\circ(B)$ as defined by Eq. (2). If B is an anion, the thermochemistry of reaction (1) reflects gas-phase acidities, which have been also tabulated [8].

$$H^+ + B \rightarrow BH^+ \tag{1}$$

$$GB = -\Delta G_1^\circ, \qquad PA = -\Delta H_1^\circ$$

$$S_p^\circ(B) = S^\circ(BH^+) - S^\circ(B) = \Delta S_1^\circ + S^\circ(H^+) = \frac{GB(B) - PA(B)}{T} + S^\circ(H^+) \tag{2}$$

The absolute PAs of bases can be obtained from threshold dissociation energies for reactions that form BH^+ from neutral precursors. These data, in conjunction with neutral thermochemistry, allow calculating $\Delta H_f^\circ(BH^+)$ which yields PA(B) using Eq. (3).

$$PA(B) = \Delta H_f^\circ(B) + \Delta H_f^\circ(H^+) - \Delta H_f^\circ(BH^+) \tag{3}$$

Such measurements define the PAs of primary reference standards to which other bases can be related through proton-transfer equilibria (4). The equilibrium constants yield the relative GBs (Eqs. (5) and (6)), and relative PAs are obtained from temperature studies using Eq. (7). Networks of these values can yield extensive thermochemical ladders.

$$B_1H^+ + B_2 \rightarrow B_2H^+ + B_1 \tag{4}$$

$$K_4 = \frac{[B_2H^+]P(B_1)}{[B_1H^+]P(B_2)} \tag{5}$$

$$-RT\ln K_4 = \Delta G_4^\circ = \Delta H_4^\circ - T\Delta S_4^\circ = GB(B_1) - GB(B_2) \tag{6}$$

$$\frac{d\ln K_4}{dT} = \frac{-\Delta H_4^\circ}{RT} = \frac{PA(B_2) - PA(B_1)}{RT} \tag{7}$$

The temperature dependence of proton affinities can be obtained [1] by differentiating Eq. (3) with respect to T (Eq. (8)):

$$\frac{d\,PA(B)}{dT} = C_p(H^+) + C_p(B) - C_p(BH^+) \tag{8}$$

Here C_p is the molar heat capacity at constant pressure. Most of the temperature dependence of absolute PA values results from the $C_p(H^+) = (5/2)R$ term, as the difference between $C_p(B)$ and $C_p(BH^+)$ in the last two terms is usually small. Moreover, this small difference is usually comparable for most bases B, and therefore the relative proton affinities of bases are essentially independent of temperature in the usual range of interest between 298 and 600 K [1]. In fact, no curvatures of van't Hoff plots were reported that would reflect measurable changes of relative PA values in equilibrium pairs.

The methods used in most equilibrium PA studies are ion cyclotron resonance (ICR) or pulsed high pressure mass spectrometry (PHPMS), both time-resolved methods where the approach to equilibrium can be observed directly. Selected ion flow tube (SIFT) mass spectrometry has been also applied [9]. The ease of variable temperature studies with PHPMS was used

in early studies to obtain relative PAs and S_p values [7,10]. Qualitatively, the order of PAs of bases can be obtained from bracketing experiments or from the dissociation of proton-bound dimers. All the experimental methods have been reviewed [11].

The concept of proton affinity applies to any species that can be protonated, including stable molecules, as well as atoms, radicals and even clusters, nanoparticles and solid surfaces. The present review concerns the GBs and PAs of stable molecules where proton attachment is often the only way to form the protonated species.

2. Historical summary

The significance of intrinsic molecular acid–base properties prompted intensive and prolonged research, starting in the 1960s when mass spectrometric methods became available, and continuing to date.

The first major compendium of GB and derived PA data by Aue and Bowers in 1979 summarized the prior history and included data on over 300 bases [12]. The earliest PA determination was attributed to Tal'roze and Frankevich in 1956, who bracketed PA(H_2O) between 163 and 172 kcal mol^{-1} using high pressure mass spectrometry (HPMS) [13] (current value 165 kcal mol^{-1}) [1]. Other early measurements included qualitative bracketing of the PAs of amines by Munson also by HPMS [14], while Beauchamp and Buttrill [15] and Brauman and Blair [16] used ICR to bracket the PAs of organic bases. The latter classical study showed that increasing methyl substitution increases the PAs of amines systematically, and that the irregular order in solution is caused by solvation effects.

Quantitative measurements of proton-transfer equilibria were first carried out by Aue and coworkers using an ICR drift cell [17]. The groups of Beauchamp and of Taft used trapped ICR cells developed by McIver [18]. The Taft group accumulated a large set of interconnected data that were analysed and reviewed [6]. Much of the early data has been incorporated in the current PA scale, or used as checks for the current scale, after a temperature correction that was needed in the early ICR data [1].

Well-defined temperatures and collisional thermalization of the ions are obtained by high pressure methods that operate in the Torr range, first applied in ion chemistry by Munson and by Field et al. [19]. Ions are also thermalized at well-defined temperatures in flowing afterglow (FA) or SIFT studies that usually operate at 0.2–0.4 Torr, which were applied by Bohme to equilibrium studies in the lower PA range [10].

A significant advance in the high pressure methods was the introduction of time-resolved, PHPMS by Kebarle that allowed verifying equilibrium in transfer and association reactions, as well as kinetic measurements over a wide temperature range [20]. Both ICR and PHPMS can verify the achievement of equilibrium by showing that B_1H^+/B_2H^+ in reaction (4) reaches a constant ratio with reaction time. Kebarle's group applied PHPMS to establish an extensive GB ladder, using measurements at 600 K to avoid clustering at lower temperatures [7,8]. Moreover, the temperature can be varied in PHPMS sources, with measurements reported from 20 to 650 K, allowing temperature studies to determine relative PAs according to Eq. (7). The method was soon adopted by Field and Meot-Ner and coworkers by pulsing the original high-pressure mass spectrometer for time-resolved studies and applying it to ion thermochemistry [21].

The body of data from ICR, FA and PHPMS studies was summarized in the 1984 NIST compendium by Lias et al. [22]. The majority of the data in this and earlier tabulations resulted from relative GB values measured at a single temperature. The PAs were calculated from Eq. (6) by assigning $S_p = R\ln(\sigma(B)/\sigma(BH^+))$. However, protonation may lead to larger entropy changes as discussed below, especially in structurally complex molecules. These uncertainties prompted the construction of a PA ladder by Meot-Ner (Mautner) and Sieck using directly measured ΔH_4° from temperature studies [2]. This study did not find significant unexpected entropy effects, but showed that the then accepted PA difference between i-C_4H_8 and NH_3, which is commonly used as

reference, needed to be expanded by 4 kcal mol^{-1} [2]. The measured relative PAs by Mau/Sieck were anchored to the prevailing PA(*i*-C_4H_8) = 195.9 kcal mol^{-1}, and using this, the results indicated that PAs in the entire upper range should be raised by 4 kcal mol^{-1} if the value used for PA(*i*-C_4H_8) was correct. However, earlier bracketing experiments from the same laboratory already suggested that the reference value of *i*-C_4H_8 should be lowered by about 4 kcal mol^{-1} [23], which was further confirmed by the equilibrium ladder of Szu/McM [3] and by more recent threshold measurements by Baer and coworkers [24] and by Traeger [25]. In any case, the expansion between *i*-C_4H_8 and NH_3 and the relative PAs measured by Mau/Sie were later confirmed, subject to a global adjustment as discussed below. When anchored to the new values of PA(*i*-C_4H_8) = 192.2 kcal mol^{-1} or PA(NH_3) = 204.0 kcal mol^{-1} [1] the Mau/Sie values still suggest some adjustments in the upper PA range compared with previous scales.

To check and extend the directly measured PA scale, Szulejko and McMahon [3] constructed a PA ladder extending from N_2 to *t*-$C_4H_9NH_2$ over a range of 105 kcal mol^{-1} which allowed anchoring the scale to the reliable reference values of PA(CO) = 141.9 kcal mol^{-1} and PA(C_2H_4) = 162.5 kcal mol^{-1}. However, the Mau/Sie [2] and Szu/McM [3] scales show some differences, especially in the middle range between C_3H_6 and *i*-C_4H_8. To reconcile these conflicts, Radom and coworkers performed ab initio G2 calculations of the GB, PA and S_p values for compounds over a wide PA range [4,5] and Sieck also performed a careful re-determination of some of the conflicting PAs [26]. Both of these tests found that the Mau/Sie PA scale needed to be somewhat contracted. The present paper will show how all of the previous and recent data can be integrated into a consistent scale.

A major contribution of the gas-phase data is that comparison with solution allows calculating the energetics of ion solvation. This, in turn, allows and a quantitative evaluation of solvation factors, which will be also reviewed briefly.

3. Absolute PAs from dissociation thresholds and bracketing

3.1. Threshold measurements

To anchor the PA ladders, absolute values must be established by non-equilibrium methods, usually from dissociation threshold measurements or ab initio calculations. For example, PA(C_3H_6) which is a useful anchor in the central PA range, can be obtained from the dissociation threshold of reaction (9) that forms *i*-$C_3H_7^+$ using Eqs. (10) and (11).

$$2\text{-}C_3H_7X \rightarrow s\text{-}C_3H_7^+ + X \quad (9)$$

$$H^+ + CH_3CHCH_2 \rightarrow s\text{-}C_3H_7^+ \quad (10)$$

$$\begin{aligned} PA(CH_3CHCH_2) = {} & \Delta H_f^\circ(H^+) + \Delta H_f^\circ(CH_3CHCH_2) \\ & - \Delta H_f^\circ(2\text{-}C_3H_7X) + \Delta H_f^\circ(X) \\ & - \Delta H_9^\circ \end{aligned} \quad (11)$$

The uncertainty of the absolute PA value may result from uncertainties in the dissociation thresholds due to vibrational bands and to poor signal/noise ratios near the threshold. Uncertainties are also associated with the thermochemistry of the neutrals in Eq. (10), especially the radicals X. In fact, when the PA in Eq. (11) is known, for example from equilibrium results, then Eq. (11) can determine ΔH_f° of the radicals.

Reaction (9) was studied by several research groups [27–31]. Recent measurements by Baer et al. used photoelectron–photoion coincidence (PEPICO) and gave $PA_{298}(C_3H_6)$ = 177.4 ± 0.5 kcal mol^{-1}, lower by 2.2 kcal mol^{-1} than the tabulated value [1], but in excellent agreement with the equilibrium and ab initio values summarized in Table 4. The absolute standards recommended by Hunter and Lias [1] include photofragmentation thresholds by the Berkowitz and Traeger groups, PEPICO data by Baer and coworkers, and ab initio data by the Dixon, Pople and Radom research groups, as summarized in Table 1. The status of the primary standards was discussed in recent papers [1,3].

Table 1 illustrates some main features of the reference values. Over a range of 68 kcal mol^{-1} most are

Table 1
Protonation thermochemistry of primary absolute reference compounds at 298 K in the NIST tabulation[a] [1]

Base	$\Delta H_f^\circ(BH^+)$	ΔS_p°	PA	GB	Method	Reference
NH_3	193.0	−1.5	204.0	195.7	Theory	[5]
H_2CCO	157.0 (0.4)	0.6	197.3 (0.7)	189.7	PI ($(CH_3)_2CO$)	[31]
i-C_4H_8	170.0 (0.3)	4.8	191.7 (0.3)	185.4	PEPICO (*t*-C_4H_9I), PI (*i*-C_4H_{10})	[24,25]
CH_3CHO	142.3 (0.1)	0.4	183.7 (0.4)	176.0	PI (C_2H_5OH)	[32,33]
CH_3CHCH_2	190.9 (0.7)	2.9	179.6 (0.7), 177.4 (0.5)	172.7	PI (2-C_3H_7Br), PEPICO (2-C_3H_7Br and 2-C_3H_7Cl)	[27–31]
H_2CO	169.3 (0.2)	2.3	170.3 (0.3)	163.3	PI (CH_3OH)	[34]
H_2S	192.3 (1.2)	1.0	168.5 (1.3)	161.0	PI $(H_2S)_2$, theory	[4,5,35,36]
H_2O	146.2	1.2	165.2 (0.7)	157.7	PI $(H_2O)_2$, theory	[4,5,37,38]
C_2H_4	215.5 (0.4)	2.8	162.6 (0.4)	155.7	PI (C_2H_5), PEPICO (C_2H_5I)	[27,28,39]
CO	197.3 (2.7)	1.0	142.0 (0.7)	134.5	PI (HCOOH), theory	[40,41]
CO_2	142.4 (0.5)	6.2	129.2 (0.5)	123.3	PI (HCOOH), theory	[41–44]

[a] Thermochemical values at 298 K, units: ΔH_f°, PA and GB in kcal mol^{-1}, $\Delta S_p = S^\circ(BH^+) - S^\circ(B)$ in cal mol^{-1} K^{-1}.

determined with uncertainties <0.8 kcal mol^{-1}. However, only three compounds are in the lower half of this range and there is a gap of 21 kcal mol^{-1} between CO_2 and C_2H_4, while the upper range is covered by seven compounds with no gap exceeding 10 kcal mol^{-1}. The highest reference compound H_2CCO lies as much as 70 kcal mol^{-1} below the bases with the highest tabulated PA values (>255 kcal mol^{-1}). To decrease the gap at the top of the ladder, a possible candidate reference compound may be CH_2CHOCH_3 (PA = 205.4 kcal mol^{-1}) whose protonated form $CH_3CHOCH_3^+$ may be obtained from the fragmentation of $CH_3CH(OCH_3)_2$. In the highest range, the PAs of alkylimines, up to 225 kcal mol^{-1} may be obtained from the fragmentation of amines such as $(CH_3)_3CNH_2 \rightarrow (CH_3)_2C = NH_2^+ + CH_3$, where the product is protonated $(CH_3)_2C = NH$ with a PA of 222.8 kcal mol^{-1}. To use these measurements, accurate thermochemistry of the neutral imines would also have to be obtained. Reference values to check the upper (PA) range can be obtained also by association and bracketing as discussed below.

3.2. Absolute PAs from bracketing

Bracketing measurements are often used to obtain relative GBs. However, in special cases, bracketing was also used to obtain absolute PA values [23], by using radicals as reference bases whose proton affinities can be calculated independently. Moreover, it was shown that for accuracy, bracketing can be refined by plotting the reaction efficiencies, which fall of as ΔG° of the proton-transfer reactions become positive, as illustrated in Fig. 1. Analogous plots were applied subsequently in the "thermokinetic method".

More quantitatively, it may be assumed that the reaction efficiency $r = k/k_{collision}$ reaches about half of its maximum value when $\Delta G^\circ = 0$ (or approximately when $\Delta H^\circ = 0$), and therefore from Fig. 1, PA(Et_2CO) = PA($C_6H_5CH_2^\bullet$) = 198.7 kcal mol^{-1}. Using the relative PA values in Table 4, this gives PA(NH_3) = 202.8 kcal mol^{-1} and PA(*i*-C_4H_8) = 190.8 kcal mol^{-1}, lower by 1.2 kcal mol^{-1} than the values from the ladders, but within the uncertainty of ±1.6 kcal mol^{-1} in $\Delta H_f^\circ(C_6H_5CH_2^\bullet)$ [1] that enters the PA calculations. Similar results in Fig. 1b yield PA(4-MePyridine) = PA($C_6H_5NH^\bullet$) = 227.0 kcal mol^{-1} in good agreement with 226.4 kcal mol^{-1} from equilibrium values [1]. Since the PAs of the reference radicals are obtained from neutral bond dissociation energies and IPs, these data provide independent PA reference values for the upper PA range.

Conversely, using the PAs of the bracketing bases in Fig. 1 from equilibrium data, the method can be used to derive the PAs of the radicals as PA($C_6H_5CH_2^\bullet$) = 199.9 kcal mol^{-1} and PA($C_6H_5NH^\bullet$) = 226.4 kcal mol^{-1}. Using auxiliary thermochemical data, these values allow calculating the IPs of the radicals or

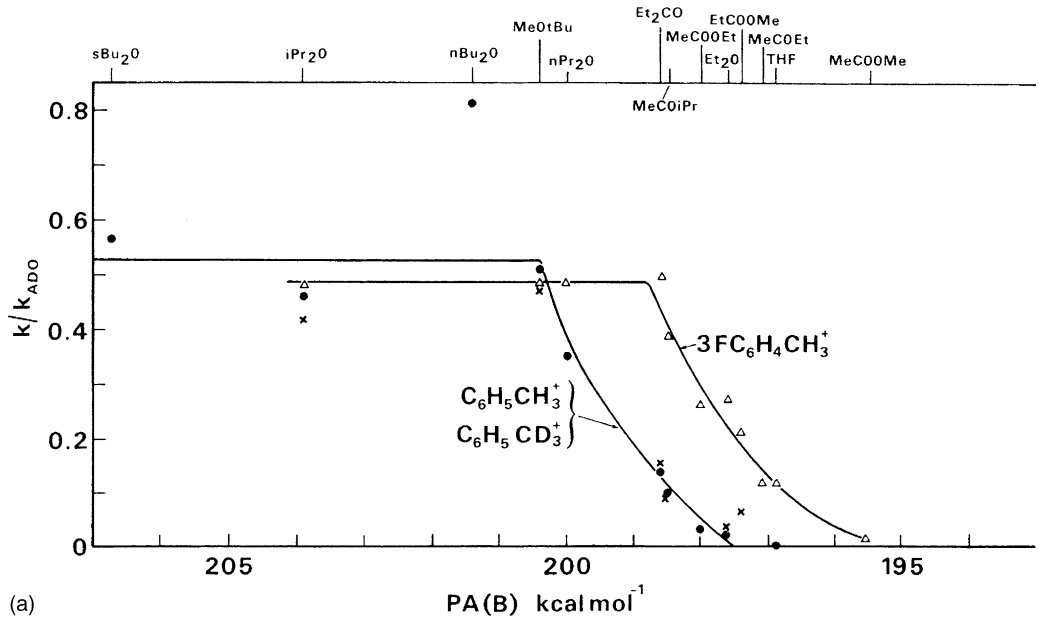

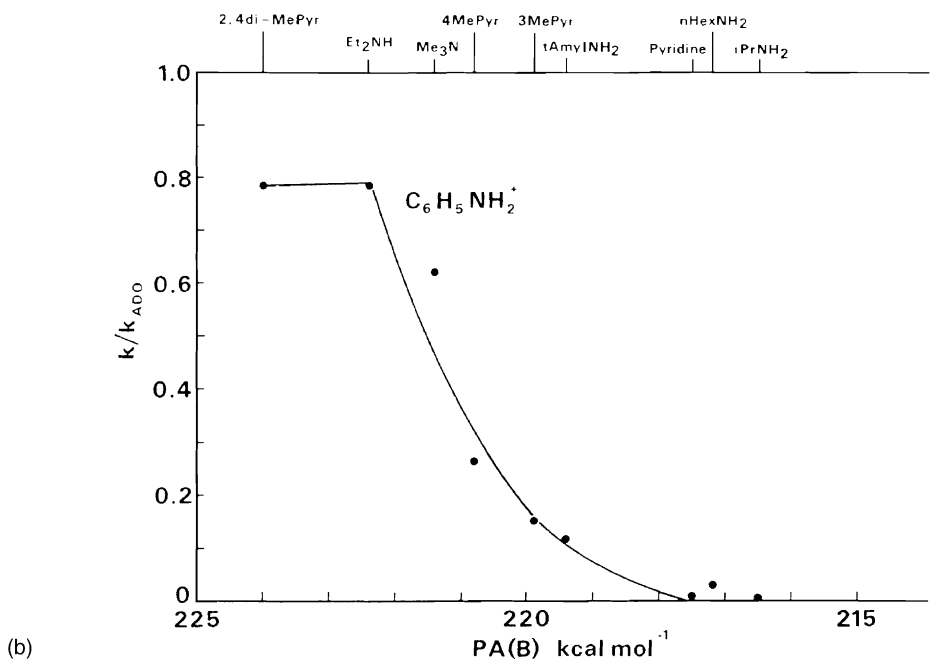

Fig. 1. Reaction efficiencies of proton-transfer (a) from $C_6H_5CH_3^{+\bullet}$ and 3-F-$C_6H_4CH_3^{+\bullet}$ to oxygen bases and (b) from $C_6H_5NH_2^{+\bullet}$ to nitrogen bases. The neutral bases are indicated on the upper abscissa [23].

the bond dissociation energies $D^\circ(C_6H_5CH_2–H)$ and $D^\circ(C_6H_5NH–H)$ with an accuracy comparable to spectroscopic determinations for these complex species.

4. Sources of error in relative GBs and PAs from equilibrium studies

The absolute reference values above may be used to anchor ladders of relative PAs and GBs from proton-transfer equilibria (4) and Eqs. (5)–(7). Uncertainties in the equilibrium measurements have been discussed in detail [2,45]. The equilibrium constants from Eq. (3) and derived ΔGB values from Eq. (4) involve uncertainties due to several sources.

a. Uncertainties in the measured signal intensities and the corresponding ion number densities in Eq. (4), for example, due to noise or errors in small ion signals. This can be significant in particular for large K values where the small ion signal $I(B_1H^+)$ and the large signal $I(B_2H^+)$ may be on opposite ends of the dynamic range. In addition, systematic errors may arise due to mass discrimination, although this can be usually calibrated.
b. Uncertainties in the partial pressures of the neutrals, especially for involatile or strongly adsorbing compounds, where the gas mixture in the ion chamber may differ from the nominal prepared mixture composition.
c. Uncertainties in the ion source temperatures that are used to calculate $\Delta G^\circ = -RT\ln K$ and $\Delta S^\circ = (\Delta H^\circ - \Delta S^\circ)/T$.
d. Incomplete thermalization of the reactants or products.

   In addition, the following errors may vary with temperature and may be especially significant at the high or low ends of temperature studies. They may cause small errors in measured ΔG_4° values but may have more significant effects on the slopes of van't Hoff plots and the derived ΔH_4° values and relative proton affinities.
e. Errors in the assigned ion source temperatures, or temperature gradients in the source between the reaction zone and the point of temperature measurements. These factors are likely to increase at extreme temperatures, affecting the calculation of enthalpy changes from $\Delta H^\circ = -R(\mathrm{d}\ln K/\mathrm{d}1/T)$.
f. Incomplete equilibrium during observable reaction times. This may affect the measured K values, especially extreme temperatures where reactions with positive or negative temperature coefficients may become slow and prevent reaching equilibrium.
g. Interference by side reactions due to impurities, dissociation, clustering or rearrangement. Irreversible clustering reactions of B_1H^+ or B_2H^+ may deplete their intensities compared with the actual equilibrium values. Isomerization to non-reactive forms or ion pyrolysis may also distort the measured K_4. While the reactions may deplete either B_1H^+ or B_2H^+ preferentially, reaction cycles may keep the ratio B_2H^+/B_1H^+ constant with time at a non-equilibrium value due to steady-state kinetics. For example, fragments produced by ion pyrolysis may protonate the neutrals and re-generate B_1H^+ or B_2H^+ resulting in steady states that appear as equilibria. Isomerization of ions may create similar artefacts. The errors introduced by these factors depend on the relative rates of the side reactions compared with the equilibrium reaction. The kinetic factors can vary with temperature as clustering is fast at low, while isomerization and pyrolysis are fast at high temperatures. These effects were analyzed and illustrated by examples [45].

The sources of error due to factors *a* and *b* above affect the values of ΔG° but not ΔH° if they are independent of temperature. Factors *e–g* often vary with temperature and may be prominent at the low or high ends of temperature studies. They may affect the ΔH° values from temperature studies more than the ΔG° measured at intermediate temperatures where the artefacts are small.

The primary source of systematic errors appears to be associated with temperature measurements. For example, in the early ICR instruments the ionizing filament created temperature gradients and the overall effective temperature in the reaction cell was

significantly higher than the nominal 300 K. Comparisons with other data [1] showed that the ΔG° of Taft require expansion by a factor of 320/300 below H_2O and 350/300 above H_2O due to this effect.

In PHPMS reaction chambers, the gas equilibrates thermally with the interior walls of the reaction chamber and especially with the surface near the ion exit pinhole or slit where the last thermal adjustment occurs before analysis. Errors may occur if the temperature is measured at a different point or if the gas does not equilibrate thermally with the walls of the ion source. For example, ΔG°_4 (600 K) values of Kebarle and coworkers [7,8] were found to fit the general GB scales better if expanded by a factor of 650/600 suggesting an apparently higher effective temperature than the nominal value [1]. On the other hand, depending on the location of the source heater, T measured at the outer wall of a reaction chamber may be lower than the heated interior walls where equilibrium occurs. This gradient would increase with increasing temperature and affect the slopes of van't Hoff plots.

For example, the variable temperature measurements of Mau/Sie were conducted by decreasing the temperature stepwise using a cooling tube through the ion source block. The temperature was allowed to equilibrate for 3–5 min at each temperature before measurement. An expansion of the PA scale could occur if the parts of the ion source where final equilibrium occurs were lower at each step by 2% than the measured value. Indeed, the measurements of Sieck using the same apparatus but much longer thermal equilibration eliminated the expansion of the PA scale [26].

The magnitude of potential errors due to temperature measurements are illustrated by the following examples. The correction of the early ICR results as suggested by Hunter and Lias [1] by a factor of 350/300 introduces a change of 18% error in ΔGB. Correspondingly, the GB span from H_2O to $(CH_3)_3N$ need to be expanded by 10.3 kcal mol^{-1}, an effect larger by an order of magnitude than the uncertainty ascribed to the final integrated PA scale below.

In PHPMS measurements, assume that in a temperature study T is measured accurately at 300 K but with a 2% error as 490 K instead of the actual 500 K. For a reaction with a true $\Delta H^\circ = -20$ kcal mol^{-1} and $\Delta S^\circ = 0$ cal mol^{-1} K^{-1}, the assigned values at 500 K would be $\Delta G^\circ = -19.6$ kcal mol^{-1}, $\Delta H^\circ = -20.6$ kcal mol^{-1} and $\Delta S^\circ = -2.1$ cal mol^{-1} K^{-1}. These errors are comparable to the usual uncertainties. As another example, an expansion in the experimental GB scale by 4% (see below) would result if the temperature assigned as 660 K was in fact 674 K, i.e., higher by 2% than the nominal value. A compression in the GB scale of Szu/McM as discussed below could result from a temperature difference of comparable magnitude in the opposite direction.

For testing these effects, a ladder of ionization energies was constructed for aromatics with known spectroscopic IPs, but the results did not show a systematic expansion [45]. Given the experimental uncertainties, it is important to test the consistency of thermochemical values also by measuring equilibrium constants at varying pressures and compositions, comparing results from various laboratories and instruments, comparing results from alternate pathways through the ladders, comparing absolute standards and theoretical values to the ladders, and comparing the derived entropies with isoelectronic neutrals or with theory.

An important conclusion form the above considerations is that the sources of error in the PHPMS GB and PA measurements are largely independent from each other even when obtained in the same experiments. Therefore, the PHPMS GB and PA scales can be considered as largely independent sources of data.

5. Relative GBs and PAs from bracketing and from the kinetic method

Equilibrium cannot always be achieved during observable reaction times. Equilibrium constants may be determined then from the ratio of the forward and reverse rate coefficients measured by ICR or SIFT. If equilibrium constants still cannot be obtained, such as for unstable or involatile molecules, the order of gas-phase basicites can be obtained by bracketing from reaction kinetics.

The bracketing method relies on fast reactions where the efficiency $r = k/k_{collision}$ is near unity. In the first applications, it was assumed that reactions are fast in the exothermic direction ($\Delta H^\circ < 0$). However, Bohme et al. [9] showed that rate coefficients are related to ΔG°, as of course it follows from the relation $\exp(-\Delta G_4^\circ/RT) = K_4 = k_4/k_{-4}$ that the fast direction is determined by ΔG°.

The relation between kinetics and thermochemistry in fast reactions was formulated more generally by Meot-Ner (Mautner) [46] as follows. "Intrinsically fast reactions" obey Eq. (12) in that they are fast in the forward direction where $\Delta G^\circ < 0$ and are slowed in the reverse direction only to the degree required by the thermochemistry. These relations include reactions with ΔG° values near zero, where $r < 1$ applies in both directions. It was observed that such kinetics results when the energy barrier is negligible [46].

$$r_4 + r_{-4} \approx 1 \tag{12}$$

$$K_4 \approx \frac{r_4}{r_{-4}} \tag{13}$$

$$r = \frac{K}{1+K} = \frac{1}{1+\exp(\Delta G/RT)} \tag{14}$$

We observed that Eqs. (12)–(14) apply in reactions with various combinations of ΔG° and ΔH°, in charge transfer and proton-transfer, and in reactions involving anions and cations. The results demonstrated, for example, that significantly endothermic reactions ($\Delta H^\circ > 0$) can be nevertheless fast if large entropy changes render $\Delta G^\circ < 0$; we observed similar behavior previously in the reactions of polyfunctional ions with internal hydrogen bonds [47] and in charge transfer reactions [48]. These observations demonstrate that bracketing reactions measure relative GBs rather than PAs. This is particularly significant in applying bracketing experiments to the GBs biomolecules, as demonstrated by Gorman and Amster [49], which commonly involve large entropy effects due to intramolecular hydrogen bonding.

Subsequently, Bouchoux and coworkers [50,51] used the rearranged form of Eq. (14) in the "thermokinetic method". In this application ΔG represented the combined energy $\Delta G^\circ_{reaction} + \Delta G^\circ_a$ but the added energy barrier term ΔG°_a is small, comparable to RT for most proton-transfer reactions [49], which supports the conditions proposed earlier for intrinsically fast kinetics [46]. Bouchoux and coworkers [50,51] applied these relations in several series of reactions to measure GBs and derived PAs such as $H_2C{=}C{=}O$ $(195.3 \pm 0.7)\,kcal\,mol^{-1}$ and $H_2C{=}NH$ $(205.5 \pm 1.2)\,kcal\,mol^{-1}$, in reasonable agreement with theory [5]. The authors also derived the thermochemistry of these unstable molecules from these measurements.

Relative GBs may be also determined applying the kinetic method to the collisional, metastable [52,53] or black-body infrared dissociation [54,55] of proton-bound dimers $B_1H^+\cdots B_2$, where the component with the higher GB retains the proton preferentially. This method is particularly useful for involatile compounds where equilibrium measurements are impractical, but whose dimers can be generated by laser desorption or electrospray. Again, the product distribution ratios B_1H^+/B_2H^+ reflect the relative GBs rather than PAs of the components. If the entropy changes in the two channels are similar and reverse barriers are absent, the product ratio is related to the relative energies of the product ions, reflecting the relative PAs of the components. The kinetic and thermokineic methods were reviewed briefly by Hun/Lia and results from these measurements were included in the NIST Tables [1].

6. Properties of thermochemical ladders

The combined PA ladders Mau/Sie [2] and Szu/McM [3] in Fig. 2 illustrate the properties of thermochemical ladders.

- The ladders provide a network of redundant overlapping paths between any two molecules, which decreases the uncertainty in the relative GBs or PAs. If two compounds are connected through n alternative paths, the uncertainty is decreased by a factor of $n^{-1/2}$ vs. the uncertainty of a single measurement. The ladders require complex iterative optimization to assign the best GB or PA values.

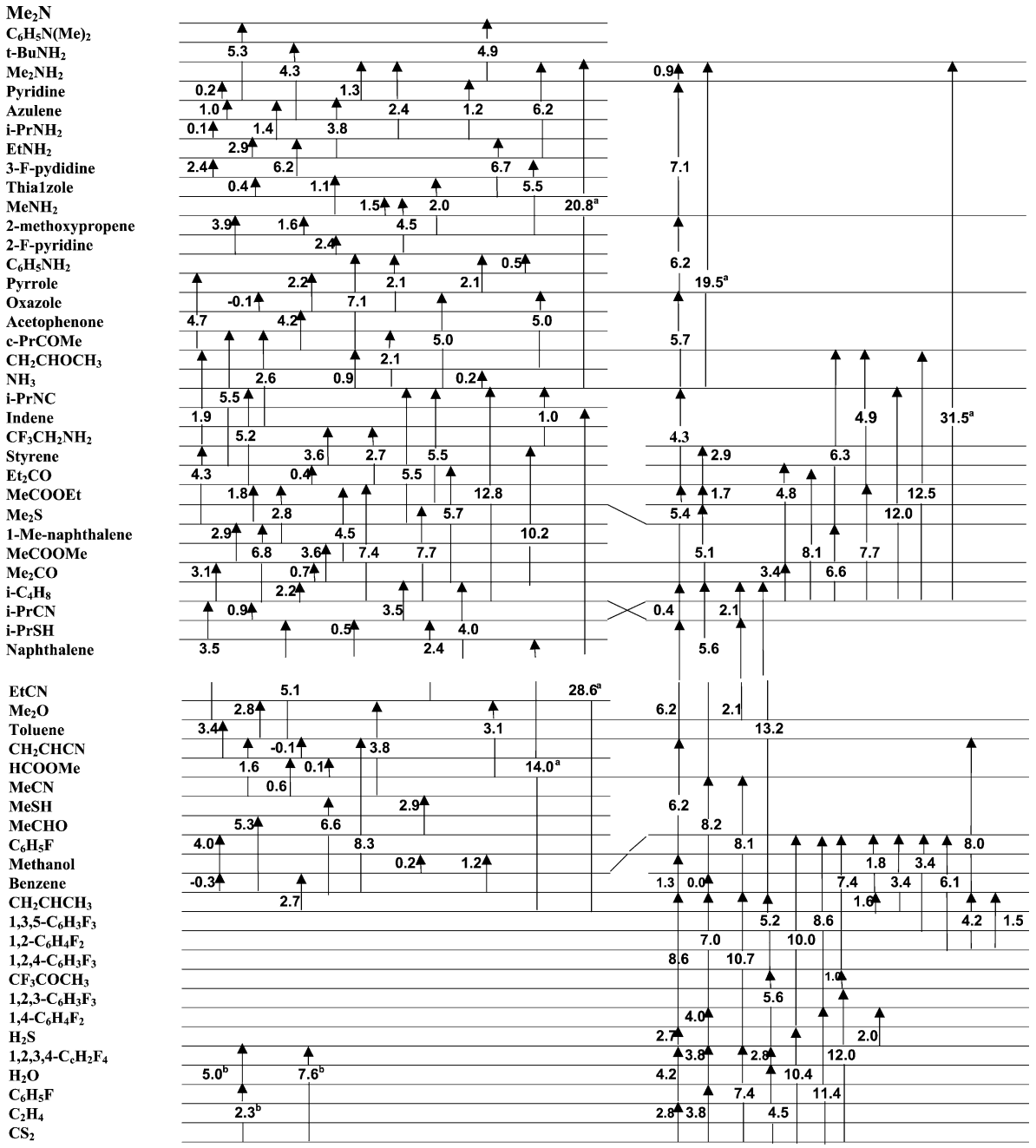

Fig. 2. Enthalpies of proton-transfer equilibria (kcal mol^{-1}) from Meot-Ner (Mautner) and Sieck [2], left-hand ladder, and from Szulejko and McMahon [3], right-hand side equilibria. (a) Results from association equilibria. (b) Results by Mautner and Field [10]. Bottom part of the Szu/McM ladder not shown.

- The uncertainty in ΔBG or ΔPA between any two compounds increases with the number of steps that connect them, due to cumulative error. Large PA differences may require several connecting steps.
- Thermochemical ladders anchor relative GBs and PAs to absolute standards. Preferred standards should be highly accurate so that they don't introduce significant external errors into the ladders. Other compounds should be connected to them by the fewest possible steps and in several redundant ways. For this reason, it is advantageous to use local standards in various ranges of the ladders. Comparing the distance between absolute standards from spectroscopy and from the equilibrium ladder tests the accuracies of both the spectroscopic and equilibrium measurements.
- Thermochemical ladders can accentuate systematic errors that lead to the contraction or expansion of the experimental scales as illustrated below.

The PA scale can be divided into lower, middle and upper part. The low PA range below H_2O (<165 kcal mol^{-1}) contains mostly small molecules including several useful independent standards such as CO, CO_2 and C_2H_4 and other important small molecules in astrochemistry such as H_2, CH_4, CO, N_2, NO and H_2O. However, relatively few molecules are in this range, allowing only a limited number of overlapping paths in the ladder.

The middle range from H_2O to NH_3 (165–204 kcal mol^{-1}) contains a larger density of various compounds. Independent standards in this range include H_2S, H_2CO, H_2CCO, CH_3CHCH_2 and *i*-C_4H_8. The lower section of this range includes astrochemical molecules such as H_2CO, H_2S and HCN, and the upper part includes representatives of many major organic classes such as alcohols, ethers, ketones, aldehydes, carboxylic acids and esters, and their sulfur counterparts, as well aromatics such as benzene, alkylbenzenes, halobenzenes and polycyclics.

The upper PA range above NH_3 (>204.0 kcal mol^{-1}) does not contain independent standards over a span of 70 kcal mol^{-1} to the top of the current PA Tables. However, the bracketing reactions in the previous section and association reactions below support the assigned values from the ladders. This range contains many nitrogen compounds that allows a dense interlocking ladder as in Fig. 2. It also includes aliphatic and aromatics amines, larger polycyclic hydrocarbons, and many polyfunctional and biomolecules whose PAs are increased by internal hydrogen bonding.

7. Tests of thermochemical ladders: charge transfer equilibria

An equilibrium ladder of charge transfer reactions involving 14 aromatic hydrocarbons was constructed to test the accuracy of thermochemical ladders in which ΔH° values are obtained from temperature studies [45]. These results of the charge transfer ladders can be compared with the spectroscopic IPs of these compounds. Although they reflect vertical IPs at 0 K, extrapolation to the 300–600 K range of the equilibrium results is less than 0.5 kcal mol^{-1} [56].

The IP ladder from 1,2,3,5-$C_6H_2(CH_3)_4$ to C_6F_6 spanned 40.7 kcal mol^{-1} in the measured $\Delta H^\circ_{\text{ionization}}$ and 40.3 kcal mol^{-1} in the ΔG°_{600} values, in reasonable agreement with the spectroscopic IP difference of 42.3 kcal mol^{-1}. The PHPMS measurements were also consistent with ICR equilibrium values that are available through part of the range [56]. For the individual reactions in the ladder, the standard deviations of the slopes and intercepts from the scatter of the van't Hoff plots and reproducibility among replicate runs were ±1 kcal mol^{-1} for ΔH° and ±2 cal mol^{-1} K^{-1} for ΔS°, similar to proton-transfer measurements. The average difference between $\Delta H^\circ_{\text{ionization}}$ between pairs of compounds and the respective spectroscopic IPs was ±0.6 kcal mol^{-1}.

For a general estimate of error in thermochemical ladders, note that two compounds may be connected by *n* steps, usually through *m* alternative parallel paths. If h° is the random uncertainty in a single step, the uncertainty of a single path of *n* steps connecting two compounds is $n^{1/2}\,h^\circ$. One effect is that small errors in individual steps can accumulate to larger errors in multiple steps. If there are *m* independent parallel paths

between the two compounds, the random uncertainty is reduced by a factor of $m^{-1/2}$ to a cumulative error of $(n/m)^{1/2}\,h^\circ$. Of cause systematic errors such as an expansion or contraction of each step by a factor f accumulate linearly to $f\,\Delta G^\circ$ which may be a significant number for two compounds separated by a large GB difference. This effect is not reduced by parallel paths. It can be large enough so that a systematic error that is undetectable in a single step becomes easily detected in an extended ladder as illustrated below.

For example, the thermochemical ladders can be obtained considering that the ladder was by 7–12 steps in several alternative paths. To combine the uncertainties in the ladder, if h° is the uncertainty in a single step, the uncertainty of a single path of n steps connecting two compounds is $n^{1/2}\,h^\circ$. For an average of 10 steps the expected cumulative uncertainty is $\pm 10^{1/2} \times 0.6 = \pm 1.9\,\text{kcal mol}^{-1}$ over the $\Delta H^\circ_{\text{ionization}}$ span of $53.1\,\text{kcal mol}^{-1}$ of the charge transfer ladders. In comparison, the measured $\Delta H^\circ_{\text{ionization}}$ span between the ends of a ladder is smaller by $2.0\,\text{kcal mol}^{-1}$ and the ΔG° span is smaller by $2.5\,\text{kcal mol}^{-1}$ than the spectroscopic span. For a ladder of 10 steps this yields an estimated uncertainty of $2.0/10^{1/2} = \pm 0.6\,\text{kcal mol}^{-1}$ per step in the measured $\Delta H^\circ_{\text{ionization}}$ values and $2.5/10^{1/2} = 0.8\,\text{kcal mol}^{-1}$ per step in the ΔG°_{600} values, comparable to the above error estimates.

A further charge transfer ladder was constructed for polycyclic aromatics [45]. The measured span of ΔG°_{600} (ionization) between 1,12-benzoperylene and naphthalene was covered in alternative paths containing an average of 10 steps which gave a measured span of $26.9\,\text{kcal mol}^{-1}$, larger by $1.8\,\text{kcal mol}^{-1}$ than the spectroscopic difference. This yields again an uncertainty estimate of $1.8/10^{1/2} = \pm 0.6\,\text{kcal mol}^{-1}$ in each individual equilibrium measurement.

Together these tests suggest uncertainties of $\pm 0.6\,\text{kcal mol}^{-1}$ in ΔH° and ΔG° and $\pm 1.4\,\text{cal mol}^{-1}\,\text{K}^{-1}$ in ΔS° values obtained from individual equilibrium measurements. This is comparable with our general experience and with the usual consistency of measurements for a given equilibrium from various sources. These values give a compounded uncertainty of $0.6n^{1/2}\,\text{kcal mol}^{-1}$ in ΔH° and ΔG° and $1.4n^{1/2}\,\text{cal mol}^{-1}\,\text{K}^{-1}$ in ΔS° for differences between two bases connected by n steps in a PHPMS thermochemical ladder. As noted, these uncertainties are reduced by a factor of $m^{-1/2}$ if m independent paths connect two bases.

8. The evaluation procedures of Hunter and Lias

The NIST Tables of Hunter and Lias [1] summarize the evaluated data up to 1998. Although directly measured PA and S_p values of Mau/Sie and Szu/McM were available, Hun/Lia did not use them because of inconsistencies (that will be resolved below). Rather, the evaluation was based on the ΔG° values from ICR and PHPMS measurements and the ab initio calculations of Eas/Rad [5]. The procedure of Hun/Lia is summarized as follows.

The compounds in the Eas/Rad calculations were used as primary standards. Relative GB_{350} and GB_{600} values from equilibrium data for these compounds were anchored to ammonia by using the relative GB values in the ladder to connect each base to ammonia, representing the thermochemistry of reaction (15).

$$NH_4^+ + B \rightarrow BH^+ + NH_3 \tag{15}$$

The relative experimental GB_{600} values, i.e., $\Delta G^\circ_{15(600)}$ and the respective $\Delta H^\circ_{15(298)}$ from ab initio PA values of Eas/Rad were used in Eq. (16).

$$\Delta S^\circ_{15} = \frac{\Delta H^\circ_{15(298)}(\text{theory}) - \Delta G^\circ_{15(600)}(\text{PHPMS})}{600} \tag{16}$$

It was also assumed that $\Delta H^\circ_{(298)}$(theory) is independent of temperature at 298–600 K. The resulting ΔS°_{15} was also assumed to be constant from 298 to 600 K. With these assumptions, Eq. (16) leads to Eq. (17) which is effectively the relation used by Hun/Lia to derive the GB_{350} values.

$$\begin{aligned}\Delta G^\circ_{15(350)} &= \Delta H^\circ_{15(298)}(\text{theory}) - T\,\Delta S^\circ_{15(350)} \\ &= \left(\frac{250}{600}\right)\Delta H^\circ_{15(298)}(\text{theory}) \\ &\quad + \left(\frac{350}{600}\right)\Delta G^\circ_{15(600)}(\text{PHPMS})\end{aligned} \tag{17}$$

In other words, a value derived by Hun/Lia for $\Delta G_{15(350)}$ is composed of 41.7% $\Delta H^\circ_{15(350)}$(theory) and 58.3% $\Delta G^\circ_{15(600)}$(PHPMS). This value was then compared with $\Delta G^\circ_{15(350)}$ from the ICR data of TAFT, also anchored to ammonia [6]. When consistent within 1 kcal mol^{-1}, the PA(B), GB(B) and S_p(B) used in the calculation were considered to be established, and absolute values were derived by anchoring to $GB_{350}(NH_3) = 195.8$ kcal mol^{-1} and $PA_{298}(NH_3) = 204.0$ kcal mol^{-1} [5]. The consistency can also be checked by comparing the derived PA values with ab initio results and with the relative PAs of the absolute standards from spectroscopy.

A further check was made by calculating the protonation entropies. Combined with $S_{p,350}(NH_3) = -1.5$ cal mol^{-1} K^{-1} [5], Eq. (18) yielded the $S_{p,350}$(B) values. They may be also calculated from Eq. (19) by deriving the absolute GB and PA values after anchoring to ammonia.

$$S_p(B) = \frac{\Delta H^\circ_{15} - \Delta G^\circ_{15}}{T} + S_p(NH_3) \quad (18)$$

$$S_p(B) = \frac{GB(B) - PA(B)}{T} + S^\circ(H^+) \quad (19)$$

The resulting S_p values were compared with the theoretical S_p values of Eas/Rad, and also examined as to reasonableness in terms of structural effects and when possible, by equating $S^\circ(BH^+)$ with the entropies of isoelectronic neutrals.

In effect, the procedure yielded composite values from relative GB values from PHPMS and the ab initio absolute PA values, which were also checked against the ICR results. The results test the internal and mutual consistencies of these scales. More details of the procedure, and applications to sample molecules are given by Hun/Lia [1].

9. GB and PA ladders and adjustments

9.1. Gas-phase basicities

As noted, Hun/Lia [1] did not use the experimental PA and S_p values by Mau/Sie [2] and Szu/McM [3] because of discrepancies which the calculations of Eas/Rad [5] aimed to resolve. Guided by the theoretical results, all the main PA scales can be rendered consistent, as follows.

The original and adjusted GB scales for key compounds are shown in Tables 2 and 3, for compounds where data are available from two or more of the PHPMS or ab initio sources. Both from the Tables and from Fig. 4 of Eas/Rad [5] it is evident that the Mau/Sie GB scale [2] is slightly expanded while the Szu/McM scale [3] is compressed vs. the theoretical values. For example, the difference between $GB_{600}(Me_2NH)$ and $GB_{600}(C_3H_6)$ is 44.3 and 41.9 kcal mol^{-1} in Mau/Sie [2] and Szu/McM [3], respectively vs. the calculated 43.2 kcal mol^{-1} [5]. Following such comparisons, the relative Mau/Sie relative GB values were multiplied by a factor of 0.96 and the Szu/McM relative GB values were multiplied by a factor 1.04 in the adjusted scales in Table 3. The adjusted scales were anchored to NH_3 as recommended by Hun/Lia [1]. Finally, the GB_{600} values were converted to GB_{298} values using the difference $GB_{600} - GB_{298}$ calculated by Eas/Rad [5] (see also Table 3, footnote a). Note that similar global adjustments were also applied by Hun/Lia [1] due to temperature corrections, using an adjustment by a factor of 350/300 = 1.17 adjustment for the Taft data [6] and 650/600 = 1.08 for the Kebarle/Lau GB scales [7,8].

The compressions or expansions observed in the experimental ladders would not be noted in individual equilibria. For example, in a typical equilibrium with $\Delta G^\circ = 3.0$ kcal mol^{-1} the expansion of the Mau/Sie scale or the contraction of the Szu/McM scale would change the result only by 0.12 and −0.18 kcal mol^{-1}, respectively, both within the typical 0.6 kcal mol^{-1} or 20% uncertainty. In fact, Eas/Rad [5] calculated the individual ΔG°_{600} and ΔH°_{600} values for 25 reactions in the Mau/Sie and Szu/McM ladders, and found agreement within ±1 kcal mol^{-1} for each reaction, within the combined estimated uncertainties of the experimental and theoretical values. Therefore, the experimental error would not be identified in an individual equilibrium measurement but it adds up to significant cumulative differences in the ladders.

Table 2
Relative gas-phase basicities and proton affinities at 600 K of selected compounds (kcal mol^{-1})[a]

600 K[a]	GB				PA			
	Mau/Sie	Sieck	Szu/McM	Eas/Rad	Mau/Sie	Sieck	Szu/McM	Eas/Rad
Me_3N	25.5			25.1	24.4			23.1
t-$C_4H_9NH_2$	21.3		19.8		20.9		19.9	
Me_2NH	19.9		18.9	19.4	19.5		19.0	18.5
Pyridine	20.8			19.7	19.3			18.0
$EtNH_2$	14.9			14.8	15.1			14.3
$MeNH_2$	10.7		10.9	11.6	11.3		11.9	11.2
Pyrrole	6.5		7.1	7.2	5.1		5.7	4.8
c-$C_3H_5COCH_3$	2.1		1.9		0.8		0.7	
NH_3	(0.0)		(0.0)	(0.0)	(0.0)		(0.0)	(0.0)
Et_2CO	−2.4		−1.4		−4.7		−4.2	
MeCOOEt	−3.0		−2.2		−5.3		−5.4	
Me_2S	−3.6			−2.9	−5.8			−5.9
MeCOOMe	−6.0	−6.2	−5.1		−9.1	−8.7	−8.5	
Me_2CO	−7.8	−7.6	−6.0	−7.5	−9.9	−9.4	−9.8	−10.4
i-PrCN	−10.6	−10.3	−9.2		−13.4	−12.4	−10.3	
i-C_4H_8	−9.2	−9.5	−7.7	−8.5	−12.4	−11.7	−11.8	−11.6
EtCN	−13.3	−12.9		−12.3	−15.7	−14.9		−15.1
Me_2O	−12.1		−10.5	−11.3	−16.0		−13.9	−15.4
Toluene	−14.4	−13.7	−12.8		−18.4	−17.4	−15.8	
CH_2CHCN	−16.1			−14.4	−18.9			−17.1
HCOOMe	−16.0	−15.2	−14.0	−15.1	−18.9	−18.0	−15.4	−17.6
MeCN	−17.3			−15.5	−19.7			−18.1
MeSH	−18.7			−16.6	−21.4			−18.8
MeCHO	−19.6	(−18.1)		−18.1	−22.6			−20.3
C_6H_5F	−22.6		−20.2		−25.5		−22.2	
MeOH	−22.4		−20.9	−21.4	−26.4		−21.8	−24.3
Benzene	−21.6		−19.6		−26.7		−23.5	
CH_3CHCH_2	−24.4		−23.0	−23.8	−29.1		−25.1	−26.8
H_2S			−32.7	−33.2			−34.8	−35.1
H_2O			−36.3	−37.7			−38.5	−39.7
C_2H_4			−37.4	−38.0			−40.9	−41.5
CS_2			−34.3	−35.3			−42.2	−41.5
CO			−58.7	−60.5			−61.6	−62.7
N_2O			−60.2				−65.7	
CH_4			−66.5				−73.3	
CO_2			−68.0	−70.0			−74.1	−75.6
N_2			−80.8	−83.2			−84.8	−86.5

[a] Relative GB values reported at 600 K. Relative PA values derived from ladders based on van't Hoff plots, Mau/Sie [2] mostly from measurements at 450–650 K, Sieck [26] at 520–660 K, Szu/McM [3] at temperature intervals mainly of 80–180 K about mean temperatures ranging between 334 and 620 K, mostly about 580 K. The van't Hoff plots in all studies were linear over the ranges studied indicating that the relative PAs are independent of temperature in the measured range within experimental accuracy. Theoretical values of [Eas/Rad] [5]. All values referenced to NH_3.

The adjusted PHPMS GB scales may be compared with the theoretical values and with the tabulated NIST [1] values. Table 3 shows good agreement among all the sources, with a scatter $\leq$1 kcal mol^{-1} for all compounds except a somewhat low value for MeSH by Mau/Sie [2]. Notably, this agreement also applies to compounds in the low GB range below H_2O. The only significant exception is C_3H_6 where

Table 3
Gas-phase basicities of selected compounds (kcal mol^{-1}) at 298 K

298 K	GB							
	Mau/Sie adj.[a]	Sie[b]	Szu/McM adj.[a]	Eas/Rad[c]	Hun/Lia[d]	Av.[e]	Std.[f]	$GB_{298} - GB_{600}$[a]
Me_3N	219.3			219.9	219.4	219.5	0.3	8.0
t-$C_4H_9NH_2$	216.0		216.1		215.1	215.7	0.6	8.7
Me_2NH	214.5		215.1	214.8	214.3	214.3	0.3	8.6
Pyridine	214.8			214.7	214.7	214.7	0.1	8.1
$EtNH_2$	209.8			210.3	209.8	210.0	0.3	8.7
$MeNH_2$	205.9		206.9	207.1	206.6	206.6	0.6	8.8
Pyrrole	200.8		201.9	201.7	201.7	201.5	0.5	7.8
c-$C_3H_5COCH_3$	196.9		196.8		196.7	196.8	0.1	8.0
NH_3	(195.8)		(195.8)	195.8	195.8	195.8	0.0	9.0
Et_2CO	192.1		192.9		192.9	192.6	0.5	7.6
MeCOOEt	191.7		192.3		192.3	192.1	0.3	7.8
Me_2S	190.9			191.4	191.5	191.3	0.3	7.5
MeCOOMe	188.9	189.3	189.3		189.0	189.2	0.3	7.8
Me_2CO	187.0	187.8	188.3	186.9	186.9	187.4	0.6	7.7
i-PrCN	184.6	185.4	185.2		184.7	185.0	0.4	8.0
i-C_4H_8	185.2	(185.6)	186.1	185.6	185.4	185.6	0.3	7.3
EtCN	181.9	182.7		182.3	182.4	182.3	0.4	7.9
Me_2O	182.4		183.1	182.7	182.7	182.8	0.3	7.3
Toluene	180.0	181.0	180.5		180.8	180.6	0.5	7.0
CH_2CHCN	179.1			180.2	180.1	179.8	0.6	7.8
HCOOMe	179.4	180.4	180.2	179.6	179.6	179.8	0.5	7.9
MeCN	178.1			179.2	178.8	178.8	0.6	7.9
MeSH	176.7			178.1	177.3	177.4	0.7	7.9
MeCHO	176.0	177.6		176.4	176.0	176.6	0.8	8.0
C_6H_5F	173.1		173.8		173.7	173.5	0.4	8.0
MeOH	172.7		172.4	173.1	173.2	172.8	0.3	7.4
Benzene	172.6		173.0		173.4	173.0	0.4	6.6
CH_3CHCH_2	171.2		170.7	170.9	172.7	170.9	0.2	7.8
H_2S			160.9	161.6	161.0	161.2	0.4	8.1
H_2O			157.1	157.1	157.7	157.3	0.4	8.0
C_2H_4			155.4	156.1	155.7	155.7	0.4	7.4
CS_2			157.1	157.5	157.2	157.3	0.2	6.0
CO			133.8	134.2	134.5	134.2	0.4	8.0
N_2O			131.3		131.1	131.2	0.1	7.1
CH_4			123.5		124.4	124.0	0.6	5.9
CO_2			122.4	123.0	123.3	122.9	0.5	6.3
N_2			110.2	111.0	111.0	110.8	0.5	7.4

[a] Absolute GB_{298} values derived from relative GB_{600} values in Table 2 by adjusting the relative values by a multiplier of 0.96 for [2] and 1.04 for [3] and anchoring the adjusted values to $GB_{600}(NH_3) = 186.8$ kcal mol^{-1} [5]. The values were converted to 298 K using $GB_{298} = GB_{600} - (PA_{600} - PA_{298}) - (600S_{p,600} - 298S_{p,298}) + [600S^{\circ}_{600}(H^+) - 298S^{\circ}_{298}(H^+)]$ (the last term in brackets = 9.96 kcal mol^{-1}). The $PA_{600} - PA_{298}$ values used were as in Table 4. The $S_{p,298}$ and $S_{p,600}$ values used were from [5], or if not available, from $S_{p,298}$ values of [1] and estimated as $S_{p,600} = S_{p,298} + 1$ cal mol^{-1} K^{-1} based on analogous compounds from [1].

[b] Relative GB_{600} values from [26], anchored to $GB_{600}(i\text{-}C_4H_8) = 192.9$ kcal mol^{-1} [5] and converted to GB_{298} as in footnote a.

[c] [5].

[d] [1].

[e] Average of columns 2–6 (when numbers are available), except CH_3CHCH_2 average of columns 2–5.

[f] Standard deviation of columns 2–6 (when numbers are available), except CH_3CHCH_2 where standard deviation is of values in columns 2–5. Range of values for each compound is about 2 × std.

the GB_{298} value assigned by Hun/Lia is too high by about 1.6 kcal mol^{-1} compared with the average of the other values.

Table 3 also shows the average GB_{298} values. As noted, the tabulated Hun/Lia values which are included in the averages are themselves an approximate average of the theoretical and of the HPMS values. The average standard deviation of the values for a given compound from the different sources is 0.4 kcal mol^{-1} and the average range is 0.8 kcal mol^{-1}, which can be used as a measure of the uncertainty in the GB_{298} data.

9.2. Proton affinities

The unadjusted PA_{600} scales in Table 2 show somewhat larger scatter. In particular, a systematic expansion is noted in the Mau/Sie scales compared with the ab initio values (see figure 5 of [5]). This expansion was noted in the careful repeat measurements of Sieck [26]. For example, the difference between $PA_{600}(Me_2NH)$ and $PA_{600}(C_3H_6)$ is 48.6 and 44.1 kcal mol^{-1} in Mau/Sie and Szu/McM, respectively vs. the calculated 45.3 kcal mol^{-1} [5]. Following such comparisons, the Mau/Sie relative PA_{600} values [2] were multiplied by a factor of 0.94 and anchored to $PA_{600}(NH_3) = 205.3$ kcal mol^{-1} [5] in the adjusted scales. Table 2 also shows that when anchored to NH_3, the Szu/McM relative PAs [2] agree well with the theoretical values above *i*-C_4H_8, but are shifted up by an about constant 1.8 kcal mol^{-1} for the lower compounds. In other words, the compounds below *i*-C_4H_8 agree with the ab initio values when anchored to CO, while the higher compounds agree better when anchored to NH_3 as a local standard. This re-anchoring retains the PA values measured by Szu/McM [2] relative to NH_3 but increases the absolute values by 1.8 kcal mol^{-1} in this range. We note in Fig. 2 that the upper range of Szu/McM is tied to *i*-C_4H_8 by 9 links, but *i*-C_4H_8 itself is tied by only one direct and three indirect links (all through Me_2CO) to the scale below. Given the long distance and many steps between CO and *i*-C_4H_8, the use of a separate local standard for the upper scale appears reasonable. Therefore, the Szu/McM PA_{600} scale was anchored to CO for compounds below *i*-C_4H_8 and to NH_3 for the higher compounds in the adjusted scales (Table 4), except *i*-C_3H_7CN which is tied to the lower scale in the Szu/McM ladders. The adjusted PA_{600} values in the PHPMS scales were converted to PA_{298} using the theoretical difference $PA_{600} - PA_{298}$ from Eas/Rad (or as in Table 4, footnote a).

The adjusted PA_{298} can be compared in Table 4 with the theoretical and tabulated [1] values. Again, all the data show good agreement, within 0.5 kcal mol^{-1} for many compounds and within 1 kcal mol^{-1} for most. Somewhat larger differences are observed in the Hun/Lia [1] value for C_3H_6 which seems to be high by 2 kcal mol^{-1} as discussed above, and the Szu/McM [3] values for CS_2, C_2H_4 and H_2S which seem to be low by 1–2 kcal mol^{-1} compared with the other sources. Included in this general agreement are the carefully measured values of Sieck [26] which are re-anchored here to *i*-C_4H_8 while retaining the relative PA values without adjustment. Note that PA_{298}(MeCHO) in the Sieck scale agrees well with the theoretical value and also with the Hun/Lia value from spectroscopic standards, giving an additional independent absolute anchor for the PHPMS equilibrium ladders. The average standard deviation of the PA for a compound from the various sources in Table 4 is 0.4 kcal mol^{-1} and the average range is 0.8 kcal mol^{-1} which indicate the uncertainty of the PA_{298} data.

The adjustments can be justified by the properties of thermochemical ladders discussed above. They yield a remarkably good agreement among the PA scales from different experimental sources and from theory. Note again the sources of error in the measured GB and PA values in the PHPMS measurements are largely independent and therefore the two scales may be considered independent. The data therefore show an agreement among relative GBs from ICR and PHPMS, relative PAs from PHPMS, absolute GBs and PAs from theory and PAs from independent standards, as well as reasonable entropies of protonation. The agreement of the PHPMS relative PAs and derived S_p values with the Hun/Lia [1] and theory increases the confidence that averaged GB values in Table 3 and PA values in Table 4 are accurate within ±0.5 kcal mol^{-1}.

Table 4
Proton affinities of selected compounds (kcal mol^{-1}) at 298 K

298 K	PA							
	Mau/Sie adj.[a]	Sie[b]	Szu/McM adj.[a]	Eas/Rad[c]	Hun/Lia[d]	Av.[e]	Std.[f]	$PA_{600} - PA_{298}$[a]
Me_3N	227.2			227.3	226.8	227.1	0.3	1.1
t-$C_4H_9NH_2$	223.8		224.1		223.3	223.7	0.4	1.1
Me_2NH	222.5		223.2	222.7	222.2	222.6	0.4	1.1
Pyridine	222.3			222.2	222.3	222.3	0.1	1.1
$EtNH_2$	218.3			218.4	218.0	218.2	0.2	1.2
$MeNH_2$	214.7		216.0	215.3	214.9	215.2	0.6	1.2
Pyrrole	208.9		209.8	208.9	209.2	209.2	0.4	1.2
c-$C_3H_5COCH_3$	204.9		204.8		204.3	204.7	0.3	1.2
NH_3	(204.0)		(204.0)	204.0	204.0	204.0	0.0	1.3
Et_2CO	199.7		199.9		200.0	199.9	0.2	1.2
MeCOOEt	199.1		198.7		199.7	199.2	0.5	1.2
Me_2S	199.0			198.6	198.6	198.7	0.3	0.8
MeCOOMe	195.5	195.5	195.6		196.4	195.8	0.4	1.2
Me_2CO	195.1	195.1	194.6	194.0	194.1	194.6	0.5	0.9
i-PrCN	191.7	192.0	192.2		192.1	192.0	0.2	1.0
i-C_4H_8	192.1	(192.2)	192.0	192.2	191.7	192.0	0.2	1.5
EtCN	190.0	190.0		189.7	189.8	189.9	0.2	0.5
Me_2O	189.6		189.0	189.3	189.3	189.3	0.3	0.6
Toluene	186.8	186.8	186.5		187.4	186.9	0.4	1.2
CH_2CHCN	186.9			187.5	187.5	187.3	0.4	0.6
HCOOMe	186.8	186.6	187.3	187.0	187.0	186.9	0.3	0.8
MeCN	186.2	186.4		186.6	186.2	186.4	0.2	0.6
MeSH	184.3			185.6	184.8	184.9	0.7	0.9
MeCHO	183.2	184.1		184.1	183.7	183.8	0.4	0.9
C_6H_5F	180.3		180.3		180.7	180.4	0.2	1.0
MeOH	179.5		180.7	180.3	180.3	180.2	0.5	1.0
Benzene	179.2		179.0		179.3	179.2	0.2	1.0
CH_3CHCH_2	177.3		177.8	177.9	179.6	177.6	0.3	0.6
H_2S	170.1[g]		167.6	169.1	168.5	168.8	1.2	1.1
H_2O	164.7[g]		163.9	164.5	165.2	164.6	0.6	1.1
C_2H_4			161.8	163.0	162.6	162.5	0.6	0.8
CS_2	161.8[g]		160.5	163.0	163.0	162.2	1.2	0.8
CO			(141.0)	141.7	142.0	141.6	0.5	0.9
N_2O			137.0		137.5	137.2	0.3	0.8
CH_4			129.0		129.9	129.4	0.6	1.2
CO_2			128.6	128.9	129.2	128.9	0.3	0.8
N_2			118.0	118.0	118.0	118.0	0.0	0.7

[a] Absolute PA_{298} derived by adjusting the relative PA_{600} values [2] in Table 2 by a multiplier of 0.94 and anchoring the adjusted values to $PA_{600}(NH_3) = 205.3$ kcal mol^{-1} [5]. The relative PA_{600} values [3] were used without adjustment, but the PAs of i-C_4H_8 and above (except i-C_3H_7CN, see text) were anchored to $PA_{600}(NH_3) = 205.3$ kcal mol^{-1} [5], increasing the PA_{600} values of NH_3 and the compounds anchored to it by 1.8 kcal mol^{-1} compared with the original paper, while the PA values below i-C_4H_8 remained anchored to $PA_{600}(CO) = 141.9$ kcal mol^{-1}. The PA_{600} values in both scales were converted to 298 K using the difference terms $PA_{600} - PA_{298}$ from [5] or when not available, the values shown in column 9 as estimated from similar compounds.

[b] Relative PA_{600} values from [26], anchored to $PA_{600}(i\text{-}C_4H_8) = 185.0$ kcal mol^{-1} [5] and converted to PA_{298} as in footnote a.

[c] [5].

[d] [1].

[e] Average of columns 2–6 (when numbers are available), except CH_3CHCH_2 average of columns 2–5.

[f] Standard deviation of columns 2–6 (when numbers are available), except CH_3CHCH_2 where standard deviation is of values in columns 2–5. Range of values for each compound is about 2 × std.

[g] From the cycle of proton-transfer equilibria among CS_2, H_2O and H_2S [10] using the average of two equilibrium results for each compound and PA values of [5] as anchor.

10. Entropies of protonation

The entropies of protonation are expressed most conveniently in terms of the "half-reaction entropies" given by the difference in absolute entropies $S_p = S^\circ(BH^+) - S^\circ(B)$ (Eq. (2)). In most early work, S_p was approximated by changes due to rotational symmetry numbers as $S_p = R\ln(\sigma(B)/\sigma(BH^+))$. However,

Table 5
Entropies of protonation half-reactions (S_p) (cal mol^{-1} K^{-1}) at 600 K

600 K	S_p				
	Mau/Sie[a]	Sie[b]	Szu/McM[c]	Eas/Rad[d]	Isoelectronic[e]
Me_3N	0.6			2.0	
t-$C_4H_9NH_2$	−0.6		−2.0		−2.0
Me_2NH	−0.6		−1.5	0.1	0.0
Pyridine	1.2			1.6	
$EtNH_2$	−1.6			−0.5	
$MeNH_2$	−2.3		−3.0	−0.8	−1.0
Pyrrole	1.1		1.0	2.8	
c-$C_3H_5COCH_3$	0.9		2.0	1.4	
NH_3	−1.3		−1.5	−1.3	−1.5
Et_2CO	2.6		2.5		2.5
MeCOOEt	2.6		3.5		
Me_2S	2.4			3.6	
MeCOOMe	3.9	3.7	4.0		
Me_2CO	2.2	2.4	4.5	3.3	
i-PrCN	3.4	3.3	0.0		3.4
i-C_4H_8	4.1	3.2	5.5	3.9	5.5
EtCN	2.7	2.9			3.1
Me_2O	5.2		4.5	5.4	2.5
Toluene	5.4	5.7	3.0	4.8	
CH_2CHCN	3.4			3.2	
HCOOMe	3.6	4.1	0.5	2.7	
MeCN	2.7	3.0		3.0	3.0
MeSH	3.2			2.4	
MeCHO	3.7	3.7		1.9	
C_6H_5F	3.6		1.5		
MeOH	5.4		−0.5	3.5	1.5
Benzene	7.2		5.0		
CH_3CHCH_2	6.6		2.0	3.7	
H_2S			1.5	1.7	2.0
H_2O			1.5	2.1	1.5
C_2H_4			4.0	4.3	
CS_2	9.6[f]		11.0	9.0	
CO			3.0	2.3	3.0
N_2O			7.0	5.7	
CH_4			9.5	8.6	
CO_2			8.0	7.9	7.0
N_2			5.0	4.2	4.0

[a] Calculated from the unadjusted experimental relative GB_{600} and PA_{600} values, anchored to NH_3 [2].
[b] [26].
[c] [3].
[d] [5].
[e] $S_{p,500}$ values from approximating $S_p(BH^+)$ by isoelectronic neutrals [3]. $S_{p,500}$ and $S_{p,600}$ values are assumed similar. For MeCN, EtCN and *i*-PrCN, isoelectronic $S_{p,298}$ values from [1] +2 cal mol^{-1} K correction to 600 K.
[f] Average from proton-transfer equilibria vs. H_2O and H_2S, anchored to $S_{p,600}$ values from [5].

Table 6
Entropies of protonation half-reactions (S_p) (cal mol^{-1} K^{-1}) at 298 K

298 K	S_p									
	Mau/Sie[a,b]	Mau/Sie adj.[a,c]	Sie[a,d]	Szu/McM[a,e]	Szu/McM[a,f]	Eas/Rad[g]	Hun/Lia[h]	Av.[i]	Std.[j]	$S_{p,600} - S_{p,298}$[a]
Me_3N	−0.4	0.3				1.0	1.3	0.8	0.7	1.0
t-$C_4H_9NH_2$	−1.6	−0.9		−3.0	−1.1		−1.4	−1.2	0.3	1.0
Me_2NH	−1.3	−0.7		−2.2	−0.9	−0.6	−0.5	−0.6	0.2	0.7
Pyridine	0.2	0.7				0.5	0.5	0.6	0.1	1.1
$EtNH_2$	−2.3	−1.8				−1.3	−1.2	−1.4	0.3	0.7
$MeNH_2$	−3.0	−2.6		−3.7	−2.9	−1.6	−1.7	−2.2	0.7	0.7
Pyrrole	0.4	0.5		0.3	0.9	2.1	2.1	1.4	0.8	0.7
c-$C_3H_5COCH_3$	−0.1	−0.1		1.0	−0.1		0.5	0.2	0.3	1.0
NH_3	−1.5	−1.5		−1.8	−1.5	−1.5	−1.5	−1.5	0.0	0.3
Et_2CO	1.6	1.3		1.5	2.4		2.1	2.0	0.5	1.0
MeCOOEt	1.6	1.3		2.5	3.0		1.2	1.7	0.9	1.0
Me_2S	0.8	0.5				2.1	2.2	1.6	0.9	1.6
MeCOOMe	2.9	2.4	2.7	3.0	3.1	1.2	1.2	2.1	0.9	1.0
Me_2CO	1.0	0.5	1.2	3.2	3.4	2.1	2.1	1.8	1.1	1.3
i-PrCN	2.4	1.8	2.4	−1.0	−1.0		1.4	1.8	0.4	1.0
i-C_4H_8	4.0	3.4	3.2	5.5	5.0	3.9	4.8	4.1	0.8	0.0
EtCN	0.7	0.0	0.9			1.3	1.1	0.8	0.6	2.0
Me_2O	3.8	3.0		3.0	5.2	3.9	3.9	4.0	0.9	1.5
Toluene	4.4	3.6	4.8	2.0	4.9	3.8	3.8	4.2	0.6	1.0
CH_2CHCN	1.4	0.6				1.2	1.2	1.0	0.3	2.0
HCOOMe	2.1	1.2	2.6	−1.0	1.6		1.2	1.6	0.6	1.5
MeCN	0.7	−0.1	1.1			1.0	1.0	0.8	0.6	2.0
MeSH	1.7	0.8				0.9	0.8	0.8	0.0	1.6
MeCHO	2.2	1.2	2.1			0.3	0.4	1.0	0.8	1.6
C_6H_5F	2.6	1.6		0.5	2.8		1.3	1.8	0.7	1.0
MeOH	3.6	2.5		−2.3	0.1	1.7	2.2	1.6	1.1	1.8
Benzene	6.3	5.0		4.0	6.0		6.0	5.7	0.5	1.0
CH_3CHCH_2	5.3	4.0		0.7	2.4	2.4	2.9	3.0	0.9	1.3
H_2S				0.6	2.2	0.8	1.0	1.3	0.7	0.9
H_2O				0.6	2.1	1.1	1.2	1.5	0.5	0.9
C_2H_4				3.0	4.1	2.9	2.7	3.3	0.8	1.0
CS_2	8.1[k]			9.5	11.1	7.5	6.7	8.4	2.4	1.5
CO				1.6	1.3	0.9	1.0	1.0	1.1	1.4
N_2O				6.0	5.9		4.8	5.2	0.7	1.0
CH_4				8.5	7.7		7.7	8.0	0.4	1.0
CO_2				6.4	5.8	6.3	6.2	6.1	0.3	1.6
N_2				3.3	1.3	2.5	2.5	2.1	0.7	1.7

[a] Calculated from the relative GB_{600} and PA_{600} values anchored to NH_3 [5] and converted to 298 K using $S_{p,600} - S_{p,298}$ in column 11, i.e., $S_{p,298}$ (B) = [(PA_{600}(B) − PA_{600}(NH_3)) − (GB_{600}(B)–GB_{600}(NH_3))]/600 + $S_{p,600}$(NH_3) − ($S_{p,600}$(B)$_{theory}$−$S_{p,298}$(B)$_{theory}$). The last term in parentheses, listed in column 11, was obtained from $S_{p,298}$ and $S_{p,600}$ values of [5], and when not available, 1 cal mol^{-1} K^{-1} was used. The reference value is $S_{p,600}(NH_3) = -1.3$ cal mol^{-1} K^{-1} [5].

[b] From relative GB_{600} and PA_{600} values in Table 2 from [2], $S_{p,298}$ calculated as in footnote a.

[c] From relative GB_{600} values adjusted by 0.96 and relative PA_{600} values adjusted by 0.94 from [2], S_p calculated as in footnote a.

[d] From [26], re-anchored to i-C_4H_8.

[e] From [3], $S_{p,600}$ values as published.

[f] From [3], relative GB_{600} values adjusted by 1.04 and PA_{600} values for i-C_4H_8 and above re-anchored to NH_3 [5], S_p values calculated as in footnote a.

[g] [5].

[h] [1].

[i] Average of columns 3, 4, 6, 7 and 8 (when available), except CH_3CHCH_2 columns 3, 4, 6, 7.

[j] Standard deviation of columns 3, 4, 6, 7 and 8 (when available), except CH_3CHCH_2 columns 3, 4, 6, 7. The range of numbers is about 2 × std.

[k] Average from proton-transfer equilibria vs. H_2O and H_2S, anchored to $S_{p,600}$ values [5] and converted to using the $S_{p,600} - S_{p,298}$ values [5].

Table 7
Thermochemistry of protonation of additional compounds at 600 K, obtained from variable-temperature equilibrium measurements

	GB (kcal mol^{-1})[a]	PA (kcal mol^{-1})[b]	S_p (cal mol^{-1} K^{-1})[c]
$C_6H_5N(CH_3)_2$	208.6	226.5	−0.4
Azulene	206.7	222.5	3.2
i-$C_3H_7NH_2$	204.0	222.4	−1.1
3-F-pyridine	199.9	217.0	1.1
2-Methoxypropene	199.4	214.6	4.2
2-F-pyridine	195.5	212.3	1.7
$C_6H_5NH_2$	194.4	211.4	1.2
Oxazole	193.5	210.0	2.1
Acetophenone	189.8	206.9	1.0
CH_2=$CHOCH_3$	189.8	205.5	3.4
NH_3	186.8	205.3	−1.3
Indene	187.9	204.2	2.4
$C_6H_5CH_2COCH_3$	184.6	203.9	−2.5
$CF_3CH_2NH_2$	185.6	203.9	−1.0
$C_6H_5CHCH_2$	185.3	201.3	2.9
1-Me-naphthalene		198.8	
i-C4H8	178.0	193.6	3.4
Naphthalene	178.6	191.9	7.5
CF_3COCH_3	155.8	173.5	0.5
C_6HF_5	149.8	164.3	6.0
CF_3CN	144.8	159.3	7.0
C_6F_6	140.5	153.8	9.5
SO_2	135.3	150.9	6.5
$(CF_3)_2CO$	132.9	150.2	4.5
OCS	135.1	150.0	7.5
SO_2F_2	129.7	144.8	8.0
C_2H_6	125.8	142.7	5.5
Xe	104.8	120.3	10.5

[a] GBs of naphthalene and above from relative GBs of [2], anchored to NH_3 [5] and adjusted by a factor of 0.96. GBs of $C_6H_5CH_2COCH_3$ and of compounds below naphthalene from [3], anchored to CO [5] and adjusted by factor of 1.04 (see text).

[b] PAs of naphthalene and above from relative PAs of [2], adjusted by factor of 0.94 anchored to NH_3. PA of $C_6H_5CH_2COCH_3$ from [3] re-anchored to NH_3, and of compounds below naphthalene from [3] anchored to CO.

[c] Calculated from adjusted GB and PA values of [2], see text. Unadjusted GB and PA values give similar S_p values differing mostly by ± 1 cal mol^{-1} K^{-1}. S_p values for $C_6H_5CH_2COCH_3$ and for compounds below naphthalene from [3].

protonation may also create additional rotational degrees of freedom. Such entropy effects were observed in the protonation of CS_2 in early measurements by Meot-Ner (Mautner) and Field [10] and attributed to CS_2 (linear) → CS_2H^+ (bent) transition leading to an $S_{p,298}$ value of 8 ± 2 cal mol^{-1} K^{-1} (from equilibrium with H_2O), which was also confirmed by the more recent values of Szu/McM [3] and Eas/Rad [5]. Similar effects are observed in S_p(Xe) [3] and in $S_p(CO_2)$ and $S_p(N_2O)$ in Tables 5–7. Positive entropy changes are also observed in the protonation of aromatics in Tables 5–7 due to planar → non-planar transitions and loosening of the structure.

Up to the last decade, entropies of protonation were measured by temperature studies only for a few molecules, especially those with special structural effects such as polyfunctional molecules [7,48] and aromatic hydrocarbons [57]. Larger sets of S_p values became available from the PHPMS temperature studies [2,3] and from the E3 calculations which were claimed to yield S_p values accurate within ± 0.3 cal mol^{-1} K^{-1} [5].

In the experimental scales, Szu/McM [3] gave S_p values derived from measurements at 420–620 K and anchored to $S_{p,500}(CO) = 3.0$ cal mol^{-1} K^{-1}. Experimental $S_{p,600}$ values may be also derived from the

Mau/Sie [2] scales using Eq. (14), by anchoring the ΔH°_{600} and ΔG°_{600} values to NH_3, calculating S_p values relative to NH_3 and anchoring to $S_{p,600}(NH_3) = -1.3\,cal\,mol^{-1}\,K^{-1}$ [5] to obtain absolute S_p values. Alternatively, the same data can be used by using the absolute GB and PA values in Tables 3 and 4 and calculating the S_p values using Eq. (2).

Entropies derived from $S_p = (GB - PA)/T$ test the mutual consistencies of the GB and PA scales. A relative shift of GB vs. PA by 1 kcal mol^{-1} would change $S_{p,298}$ by 3.4 cal mol^{-1} K^{-1} making S_p values a sensitive probe of internal consistency among GB and PA ladders. The average std for the scatter of S_p values for a given compound from various sources in Table 6 is ±0.7 cal mol^{-1} K^{-1} and the average range is 1.5 cal mol^{-1} K^{-1}. Moreover, the data in Table 6 also agree within 2 cal mol^{-1} K^{-1} with estimates based on isoelectronic analogues (i.e., using $S_p(NH_4^+) \approx S_p(CH_4)$, $S_p(MeOH_2^+) \approx S_p(MeNH_2)$, etc.), and Eas/Rad [5] showed that such comparisons are accurate within 1.5 cal mol^{-1} K^{-1} for most compounds. This degree of accuracy of the S_p values calculated from PHPMS data shows that the GB and PA values are mutually consistent within 0.5 kcal mol^{-1} which is consistent with the above uncertainty estimates for these values.

Table 6 shows $S_{p,298}$ derived both from the original and the adjusted PHPMS data. In the Mau/Sie data [2], the $S_{p,298}$ values from the original or adjusted GB and PA scales are similar, as both scales were compressed by similar amounts. In the Szu/McM [3] data, the $S_{p,298}$ values from the adjusted scales, especially for *t*-$C_4H_9NH_2$, Me_2NH and MeOH, are more consistent with S_p values from other sources than the unadjusted values, providing further support for the adjustments.

11. Protonation thermochemistry of additional compounds

In addition to the compounds in Tables 2–6, experimental PA and S_p data are available for the additional compounds in Table 7 from the Mau/Sie or Szu/McM ladders. No theoretical data are available for these compounds, but given the accuracy of the adjusted scales above, the GB and PA values in Table 7 should also be reliable within ±1 kcal mol^{-1} and the S_p values ±2 cal mol^{-1} K^{-1}. The data are listed at 600 K as no calculations are available for conversion to 298 K, but the data may be converted to 298 K to a good approximation using the (600–298 K) conversion factors for similar compounds in Tables 3, 4 and 6.

As above, the data may be judged by the "reasonableness" of the S_p values, such as similarity with related compounds. For example, the primary amines in Table 7 show small negative S_p values, the fluoropyridines show small positive values, and the ethers show larger positive S_p values, all comparable with related compounds in Table 5. The aromatic compounds azulene, indene and styrene show large positive S_p values, with an especially the large 7.5 cal mol^{-1} K^{-1} for naphthalene, consistent with the value given by Hun/Lia [1] based on the data of Li and Stone [57]. The 2.9 cal mol^{-1} K^{-1} for styrene is similar to *i*-C_4H_8, consistent with protonation of the olefin group. Interestingly, $C_6H_5NH_2$ shows positive S_p consistent with protonation on the aromatic ring, while $C_6H_5N(CH_3)_2$ shows small negative S_p comparable to amines suggesting protonation on nitrogen. These respective potonation sites a reasonable considering the basicities of the amine groups.

The fact that the S_p values in Table 7 are consistent within 3 cal mol^{-1} K^{-1} with similar compounds implies that the GB and PA values in Table 7 from which they are derived are mutually consistent to better than 2 kcal mol^{-1}. The agreement is notable as this group contains relatively involatile compounds such as azulene, styrene and naphthalene, where inaccurate pressure assignments could have caused significant errors in GB and S_p.

12. Proton affinities from association equilibria

The association of carbonium ions with neutral molecules can lead to protonated bases. Early examples were presented in the work of Hiraoka and

Kebarle [58] in the association of $C_2H_5^+$ with CH_4 leading to $C_3H_9^+$ [58] and of $C_2H_5^+$ and *s*-$C_3H_7^+$ with H_2 leading to $C_2H_7^+$ and $C_3H_9^+$ [59], and the observations of Meot-Ner (Mautner) [60] on the association of *s*-$C_3H_7^+$ and *t*-$C_4H_9^+$ with HCN presumably leading to the protonated isocyanides *i*-$C_3H_7NCH^+$ and *t*-$C_4H_9NCH^+$. In the Mau/Sie [2] and Szu/McM [3] work, reaction (20) was measured and Eqs. (18) and (19) were applied.

$$t\text{-}C_4H_9^+ + NH_3 \rightarrow t\text{-}C_4H_9NH_4^+ \quad (20)$$

$$\Delta H_f^\circ(t\text{-}C_4H_9NH_3^+) = \Delta H_{20}^\circ + \Delta H_f^\circ(t\text{-}C_4H_9^+) + \Delta H_f^\circ(NH_3) \quad (21)$$

$$PA(t\text{-}C_4H_9NH_3) = \Delta H_f^\circ(t\text{-}C_4H_9NH_2) + \Delta H_f^\circ(H^+) - \Delta H_f^\circ(t\text{-}C_4H_9^+) - \Delta H_f^\circ(NH_3) - \Delta H_{17}^\circ \quad (22)$$

Equilibrium (20) is useful as it connects the primary standard *i*-C_4H_8 directly to *t*-$C_4H_9NH_2$ in the upper PA range, spanning a PA range over 30 kcal mol^{-1} in one step, with an uncertainty of ±1 kcal mol^{-1}, comparable or better than the cumulative uncertainties of 4–6 proton-transfer steps. The data in Table 8 lead to a PA difference of 32.6 ± 1 kcal mol^{-1} between *i*-C_4H_8 and *t*-$C_4H_9NH_2$ [2] or 31.5 kcal mol^{-1} [3], both in good agreement with 31.7±0.4 from the PA scales in Table 4.

Association reactions can yield thermochemical values that are not available from direct measurements. Examples for *i*-C_3H_7SH and *i*-C_3H_7NC are shown in Table 8. Directly measured PA by PHPMS for these compounds is impractical because of chemical complications.

The association equilibria give PA values only if the products are the covalently bonded ions. Alternatively, non-covalent clusters may form. For example, Yamdagni and Kebarle [65] reported that the association of $C_2H_5^+$ and *s*-$C_3H_7^+$ with H_2 at low temperatures yields loosely bonded clusters, while an energy barrier for condensation is overcome at higher temperatures leading the respective protonated alkanes. Forming the loose clusters usually involves an entropy change of −20 to −25 cal mol K^{-1} while covalent addition usually −30 to −40 cal mol^{-1} K^{-1}. In the association of *t*-$C_4H_9^+ + H_2O$, Meot-Ner (Mautner) et al. [61] reported that a non-covalent cluster is formed that is similar in energy to the covalent *t*-$C_4H_9OH_2^+$

Table 8
Proton affinities of neutrals RM from association equilibria of carbonium ions R^+ with neutrals $R^+ + MH \rightarrow RMH^+$

R^+	MH	RMH^+	$-\Delta H_{assoc.}^\circ$ [a]	PA(RM) [a,b]	PA(RM) lit. [a,c]
$C_2H_5^+$	H_2	$(C_2H_6)H^+$	11.8[d], 12.8[e]	161.6, 162.6	162.6
	CH_4	$(C_3H_8)H^+$	6.6[d]	143.2	149.5
s-$C_3H_7^+$	H_2S	(*s*-$C_3H_7SH)H^+$	32.0[f]	191.2	192.0
	HCN	(*s*-$C_3H_7NC)H^+$	39.6[f]	206.8	204.8
t-$C_4H_9^+$	H_2O	(*t*-$C_4H_9OH)H^+$	11.2[g]	189.9	191.8
	CH_3OH	(*t*-$C_4H_9OCH_3)H^+$	29.1[h]	205.2	201.1
	NH_3	(*t*-$C_4H_9NH_2)H^+$	46.8[f], 45.3[i]	224.8, 223.3	223.2

[a] All units kcal mol^{-1}.
[b] Calculated from association reactions as in Eqs. (17)–(19), using accessory thermochemistry from NIST Tables [http://webbook.nist.gov/chemistry]. For $\Delta H_f^\circ(i\text{-}C_3H_7^+)$ the value of 193.0 kcal mol^{-1} was used as obtained from $PA(C_3H_6)$ = 177.6 kcal mol^{-1} in Table 4.
[c] [1].
[d] [58,59].
[e] [3].
[f] [2].
[g] [87].
[h] [62].
[i] [3].

ion but of more positive entropy by 13 cal mol^{-1} K^{-1}. Subsequently, Norrmann and McMahon [62] reported that *t*-$C_4H_9^+$ can form either clusters at high temperatures or covalent adducts at low temperatures with oxygen bases, the latter allowing PA determinations (Table 8).

Association energies from various sources often vary by 1–2 kcal mol^{-1} [63] which may be assigned as the uncertainty in the derived PA values. Within these limits, satisfactory agreement is observed in Table 8 with the PA data from [1]. These association equilibria constitute a further independent source that validates the PA scales.

13. Structural effects, and intramolecular ionic hydrogen bonds

The GBs and PAs of molecules are affected by various structural factors. Attachment of the proton forms a strong covalent bond, attested by the proton bonding energies (PAs) of 100 to over 250 kcal mol^{-1}. Upon attachment to a molecule, a substantial fraction of the proton charge is transferred to the polarizable neutral. The magnitude of charge transfer from the proton and its relation to the PAs is illustrated in Fig. 3 by the structures and charge distributions in H_2O and NH_3 and their protonated counterparts.

In fact, the main molecular trend up the scale of proton affinities is the increase in polarizabilities. Small molecules with low polarizabilities are in the lower PA range while complex organics with large polarizabilities are mostly in the upper PA range. In homologous series such as alcohols, ethers, ketones, thiols and amines, the PAs increase with the sizes and polarizabilities of the alkyl substituents and with their proximity to the protonated site. In addition to this electrostatic factor, electronic effects are of course also significant, as reflected in the significance of the proton acceptor (lone pair donor) atom. For example, for organic bases with given alkyl substituent R, the PAs increase in the order PA(R_2O) < PA(R_2S) < PA(R_2NH). Electronic effects can sometimes reverse the effects of polarizabilities, as for example in the effects of fluorine substitution.

In some cases protonation may cause significant structural changes. For example, the protonation of olefins opens the double bond and creates new molecular rotors. The protonation of aromatics also opens double bonds and destroys aromatic π systems. However, in these groups too, the PA usually increases with increasing polarizability. Structural effects on the PAs

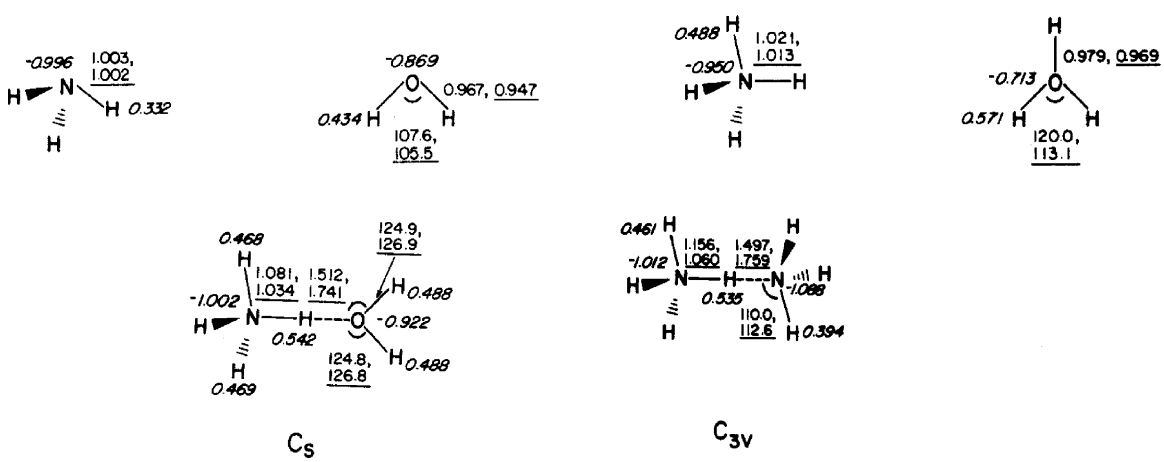

Fig. 3. Structures and Mullikan charge densities in the neutrals, protonated bases, and dimers of water and ammonia [23] for the dimers $H_3O^+\cdots OH_2$ (bond strength $\Delta H_D^\circ = 33.2 \pm 2$ kcal mol^{-1}), $NH_4^+\cdots NH_3$ (bond strength $= 22.0 \pm 2$ kcal mol^{-1}) and $NH_4^+\cdots OH_2$ ($\Delta H_D^\circ = 20.1 \pm 2$ kcal mol^{-1}). Structures from [88], bond strengths from [63].

are reviewed in more detailed in the companion article by Deakyne [64].

Particularly large structural effects are observed in polyfunctional molecules where protonation leads to the formation of cyclic structures with intramolecular ionic hydrogen bonds. This effect stabilizes the ions and increases the PAs of the molecules. Forming the internally bonded constrained structures also involves negative entropy changes comparable to the differences between linear and cyclic hydrocarbons [12]. However, the overall free energy effect is usually stabilizing, i.e., GB values increase due to the internal bond although less than the increases in the PA values.

The effect was observed first by Aue Bowers in the increased basicities of diamines [12]. Early temperature studies by Yamdagni and Kebarle [65] and by Aue et al. [66] and by Meot-Ner (Mautner) et al. [48] used proton-transfer equilibria to measure the enthalpy and entropy contributions of intramolecular IHB formation in diamines and triamines. Further studies found internal IHB effects in protonated polyethers and crown ethers [67,68], in diketones [67,69] and in dialcohols [70]. Molecules that contain two different functional groups such as amino alcohols [48] and methoxy alcohols [71] were also investigated. The cyclic structures in diamines, polyethers and methoxy alcohols were confirmed by ab initio calculations by Yamabe and coworkers [72], as illustrated in Fig. 4. The cyclic structures were also confirmed by H_2O and MeOH loss through metastable and collisional dissociation [73].

Table 9 shows the thermochemistry of representative internal bonds. Table 9 also shows the contributions of the enthalpy, entropy and free energy of the internal bonds, ΔPA_{IHB}, ΔGB_{IHB} and $\Delta S_{p,IHB}$, respectively. These terms are calculated by comparison with analogous monofunctional bases. A direct assignment of cyclisation energies can be also made computationally by calculating the energies of the linear and cyclised isomers [72]. The internal bond strengths and their contribution the PAs and GBs increase with ring size as the strain decreases and the hydrogen bond approaches optimized geometry, as observed in the diamines in Table 9. Multiple bonds and electrostatic interactions of additional polar groups can add further stabilization [68]. A remarkably large increase in the PA_{298} by 38 kcal mol^{-1} and in GB_{298} by 31.8 kcal mol^{-1} is observed due to multiple interactions in the protonation of 18-crown-6, compared with monofunctional ethers [67,68]. The dipeptide analogue CH_3O-Ala-OCH_3 in Table 9 also shows increased PA and GB due to internal bonding in the ion, but the effects are smaller due to an unoptimized, strained hydrogen bond [48].

The overall stability of the internal bond can be characterized by the temperature required to open the bond, $T_{op} = \Delta H^\circ_{IHB}/\Delta S^\circ_{IHB}$ at which half of the equilibrium ion population is in the open form [48]. Increasing ring size decreases ΔH°_{strain}, increases ΔH°_{IHB} and stabilizes the ion as expressed by T_{op} in all classes of compounds. These trends are reflected

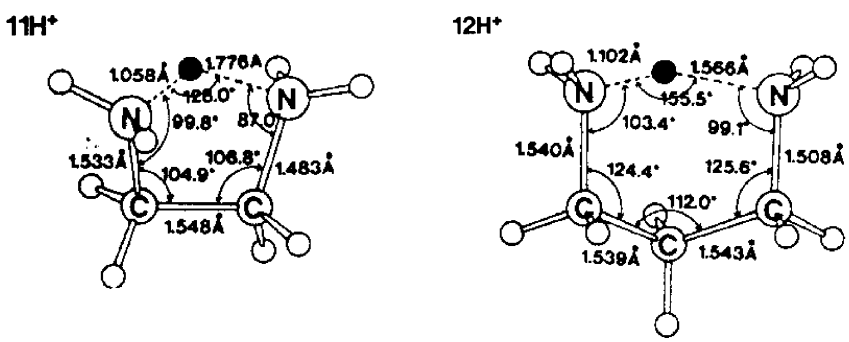

Fig. 4. Intramolecular hydrogen bonds in protonated diamines [72].

Table 9
Thermochemistry of intramolecular hydrogen bonds and their contributions to gas-phase basicity and proton affinity

Base	ΔPA_{IHB}[a]	ΔGB_{IHB}[b]	$-\Delta S_{p,IHB}$[a]	Stability (T_{op})[c]	Reference
Diamines					
$H_2N(CH_2)_2NH_2$	6.7	4.3	8.1	824	[48]
$H_2N(CH_2)_3NH_2$	14.1	9.7	14.8	952	[48]
$H_2N(CH_2)_4NH_2$	17.9	12.8	17.2	1042	[48]
Dialcolhols, diethers					
$HO(CH_2)_3OH$	19.1	14.0	17.0	1127	
$CH_3O(CH_2)_3OCH_3$	16.0	14.2	6.0	2680	
Mixed or multiple functional groups					
$H_2N(CH_2)_3OH$	8.8	5.2	12.0	740	[48]
$CH_3O(CH_2)_3OH$	17.5	13.4	14.1	1238	[71]
18-Crown-6	38.0	31.4	22.0	1728	[68]
Dipeptide analogue					
$CH_3CONHC(CH_3)COOCH_3$	6.9	2.7	14.1	492	[48]

[a] Units ΔPA_{IHB} and ΔGB_{IHB} in kcal mol^{-1}, $\Delta S_{p,IHB}$ in cal mol^{-1} K^{-1}, all at 298 K. Values represent changes due to internal bonding as derived from comparison with monofunctional molecules.
[b] Increase in GB_{298} (kcal mol^{-1}) due to IHB formation.
[c] Stability as represented by the temperature of r bond opening T_{op} $(K) = \Delta H^{\circ}_{IHB}/\Delta S^{\circ}_{IHB}$.

by increasing GB and PA with increasing ring size up to 4–6 CH_2 groups separating the hydrogen bonding groups, where the bond becomes optimized. In the examples in Table 9, T_{op} is above the thermal stability of the compounds and the internal bond will be stable at any temperature where the ion itself is stable. Intramolecular IHBs are significant in polyfunctional biomolecules as discussed below.

14. Comparison with solution basicities, and solvation factors

Comparing the gas phase and solution basicities reveals the major role of solvent effects. In classic examples, early studies by Brauman and Blair showed that the relative acidities of alcohols and basicities of amines are greatly compressed in solution vs. the gas phase [16]. For example, $\Delta H^{\circ}_{\text{proton transfer}}$ from NH_4^+ to CH_3NH_2, $(CH_3)_2NH$ and $(CH_3)_3N$ is −10.9, −18.1 and −22.8 kcal mol^{-1}, respectively [1] in the gas phase, while in aqueous solution the values are compressed or reversed to −0.7, +5.0 and +3.7 kcal mol^{-1}, respectively [6].

Bonding of ions BH^+ to solvent molecules involves partial charge transfer from the ion to the solvent as observed in the dimers in Fig. 3. The bond is efficient if the base B is weak and the charge in BH^+ remains largely localized on the proton. The basic reason for the relative solvent effects in the alkyammonium ions in Table 10 is that the protic hydrogens of NH_4^+ have larger positive charges than, for example, in Me_3NH^+, and also more protic hydrogens. Consequently, NH_4^+ bonds more strongly to a water solvent molecule than Me_3NH^+ (bonding energies of 20.6 and 14.5 kcal mol^{-1}, respectively [63]). These effects increase further as more water molecules are added as observed in Table 10. For example, the solvation energies of $MeNH_3^+$, $Me_2NH_2^+$ and Me_3NH^+ by $4H_2O$ molecules are smaller than of NH_4^+ by 9, 14 and 19 kcal mol^{-1}, respectively [74]. These values are equal within experimental accuracy to the relative solvation energies by bulk water which are smaller than those of NH_4^+ by 6, 13 and 20 kcal mol^{-1}, respectively [6].

From such analysis, it is evident that effects of ion solvation on aqueous basicities are as significant as the molecular effects. Gas-phase protonation

Table 10
Solvation thermochemistry and solvation factors of alkylammonium ions[a]

	PA(B)[b]	$\Delta H^\circ_{0,4}$ [c,d]	$\Delta H^\circ_{g\to aq}(BH^+)$ [c,e]	$-\Delta H^\circ_{dielectric}$ [c,f]	ΔH°_{cavity} [c,g]	$-\Delta H^\circ_{hydrophobic}$ [c,h]	$-\Delta H^\circ_{IHB}$ [c,i]
NH_4^+	204.0	63	87	70	7	0	23
$MeNH_3^+$	214.9	54	81	61	13	12	20
$EtNH_3^+$	218.0	57	80	55	10	17	22
$Me_2NH_2^+$	222.2	49	74	55	13	21	16
$Et_2NH_2^+$	227.6	46	72	48	17	28	17
Me_3NH^+	226.8	44	67	51	15	28	6
Et_3NH^+	234.7	37	64	44	21	37	6
$PyridineH^+$	222.3	41	66	50	16	27	10

[a] Units kcal mol^{-1}.
[b] [1].
[c] [74].
[d] Total attachment energies of $4H_2O$ molecules to BH^+.
[e] Solvation energy, i.e., enthalpy of transfer of BH^+ from gas phase to water [74] using the current PA values in Eq. (23) may vary these values by about 2 kcal mol^{-1}.
[f] Enthalpy of dielectric charging of solvent cavity.
[g] Surface enthalpy of solvent cavity.
[h] Total enthalpy of bonding of alkyl CH hydrogens to water.
[i] Total ionic hydrogen bond energies of BH^+ to solvent.

thermochemistry allows quantifying these large solvation effects, using the Born–Haber cycle [6,12,74]:

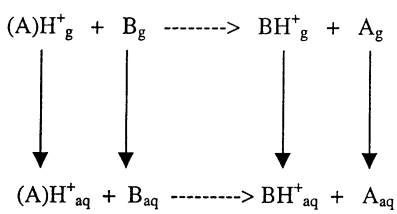

In the absence of A (reactions of bare H^+) the cycle represents absolute basicites, while when applied to protonated bases AH^+ it represents relative basicities. Of interest are the solvation energies, i.e., enthalpies of transfer from gas phase to solution of the ions, denoted as $\Delta H^\circ_{g\to aq}(BH^+)$. The relative solvation energies of A and B may be denoted as $\delta\Delta H^\circ_{g\to aq}(B)$ and of the ions as $\delta\Delta H^\circ_{g\to aq}(BH^+)$, the relative enthalpies of protonation of two bases in the gas phase as $\delta\Delta H^\circ_{prot}(B)_g$ and in solution as $\delta\Delta H^\circ_{prot}(B)_{aq}$. The thermochemical cycle then yields Eq. (23).

$$\delta\Delta H^\circ_{g\to aq}(BH^+) - \delta\Delta H^\circ_{g\to aq}(B) = \delta\Delta H^\circ_{prot}(B)_{aq} - \delta\Delta H^\circ_{prot}(B)_g \quad (23)$$

The solvation energies of the neutrals and the aqueous enthalpies of protonation are known for many molecules. Measurements of the gas-phase protonation energies therefore leaves the ion solvation energies $\delta\Delta H^\circ_{g\to aq}(BH^+)$ as the only unknown, which may be calculated from Eq. (23). Taft constructed an extensive list of ion solvation energies $\delta\Delta H^\circ_{g\to aq}(BH^+)$ relative to ammonia [6], and Table 10 shows some representative values. Free energies of solvation can be treated similarly.

Table 10 shows that the solvation energies of the ions decrease systematically with increasing alkyl substitution. A main factor is the decreasing hydrogen bond energy to the first solvent molecules as the substitution increases the PAs and the charge becomes delocalized from the B–H^+ proton to the substituents. This trend is demonstrated by the solvation energy by the first four H_2O molecules (Table 10) which nearly reproduces the decreasing bulk solvation energies.

The solvation energies can in turn be decomposed into contributing terms [74] according to Eq. (24).

$$\Delta H^\circ_{g\to aq}(BH^+) = \Delta H^\circ_{cavity} + \Delta H^\circ_{dielectric} + \Delta H^\circ_{hydrophobic} + \Delta H^\circ_{IHB} \quad (24)$$

The solvation energies are composed of the continuum terms which are the dielectric solvation of the ion charge and the surface energy of the cavity that

accommodates the ion, and the hydrogen bonding terms of the interactions of the protic (IHB) and alkyl hydrogens (hydrophobic interactions) with water.

The first two terms can be calculated from continuum models. To find the hydrophobic term, we used the solvation energy of the clusters $\Delta H^{\circ}_{g\rightarrow aq}$ ($BH^+ \cdot 4H_2O$) obtained from cluster thermochemistry and Born–Haber cycles, and an equation similar to (24) for the solvation energy of the $BH^+ \cdot 4H_2O$ cluster. The ionic contributions to hydrogen bonding are contained in the cluster binding energy, and the dielectric and cavity terms for solvating the cluster can be also calculated. The remainder of experimental solvation energy of the cluster yields the hydrophobic term. Once found, this term is then used as $\Delta H^{\circ}_{hydrophobic}(BH^+)$ for the solvation of the bare BH^+ ion itself, whose dielectric and cavity energy terms are also calculated. The remainder the experimental solvation energy $\Delta H^{\circ}_{g\rightarrow aq}(BH^+)$ identifies the ionic hydrogen bond contributions to the solvation of the ion.

The results for alkylammonium ions are illustrated in Table 10. All the terms exhibit reasonable trends. The dielectric term decreases while the cavity surface energy increases with ion size. The IHB contributions decrease with the number and acidity of protic hydrogens, while the hydrophobic term due to interactions of the alkyl hydrogens with water becomes more stabilizing with increasing alkyl substitution. These trends can be reproduced by the empirical Eqs. (25) and (26).

$$-\Delta H^{\circ}_{IHB} = a + 10n^{+}_{BH}\ \text{kcal mol}^{-1} \quad (25)$$

Here the constant a is $14\ \text{kcal mol}^{-1}$ for alkyloxonium and $-4\ \text{kcal mol}^{-1}$ for alkylammonium ions and $n_{BH}{}^{+}$ is the number of protic hydrogen on the protonated functional group.

$$-\Delta H^{\circ}_{hydrophobic} = n_{CH}(b - 0.1n_{CH}) \quad (26)$$

Here the constant b is $3.2\ \text{kcal mol}^{-1}$ for alkyloxonium and $3.0\ \text{kcal mol}^{-1}$ for alkylammonium ions, and n_{CH} is the total number of alkyl hydrogens on the substituents. Apart form the constants, each protic hydrogen contributes $10\ \text{kcal mol}^{-1}$ and each alkyl hydrogen contributes $3\ \text{kcal mol}^{-1}$ to the solvation energy. The analysis also shows special effects, for example, the inefficient solvation of aromatic ions such as pyridineH^+ due to decreased hydrophobic solvation [74].

The analysis is made possible by the gas-phase PAs and cluster thermochemistry. They allow calculating the solvation thermochemistry of the ions and resolving the complex thermochemistry of ion solvation into a few simple experiment-based and structurally reasonable terms [74]. The results allow estimating the solvation energies of further ions.

15. Gas-phase basicities of biomolecules

Ions of involatile biomolecules can be studied using matrix assisted laser desorption (MALDI) [75] or electrospray [76] to generate the ions, in combination with HPMS [77] or drift cell/ion chromatography [78,79]; collisional dissociation [52,53] or black body infrared radiative dissociation ZETRID/BIRD [54,55] and Fourier transform ion cyclotron resonance (FT-ICR) [80] to study the thermochemistry. These studies show that the phenomena observed in model molecules, such as internal and polydentate hydrogen bonds, can significantly increase the GBs of biomolecules. For example, FT-ICR bracketing showed that internal IHBs in $LysH^+$ and $(Gly\cdot Lys)H^+$ result in increased basicity [49]. As in the bifunctional molecules in Table 8, the internal IHBs in biomolecules can also be increasingly optimized with increasing size, and stabilized by additional polar groups. For example, the PAs of glycine oligomers Gly_n increase with increasing size due to interactions among polar groups in folded structures [81]. Insight into these complex systems may be obtained by cluster models of bioenergetics [82–84].

As further examples, intramolecular hydrogen bonds were observed in the di-protonated (gramicidin S)$2H^{2+}$ ion [85]. Folded conformations were also observed in dinucleotides, and the degree of hydrogen bonding in a given conformation appeared to be the primary determinant in energy [86]. The structures of singly or multiply protonated biomolecules can involve multiple internal bonds such as in Fig. 5, that contribute to the basicites.

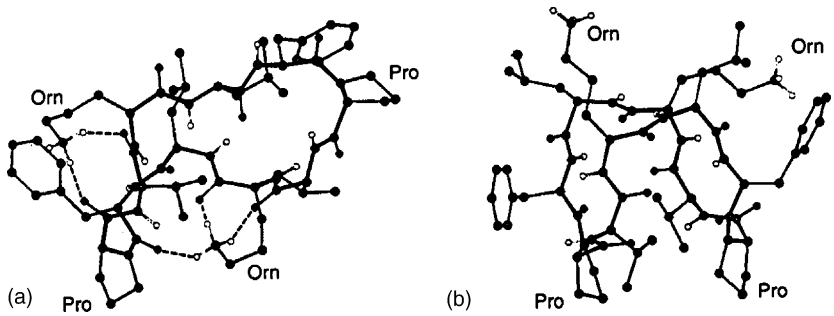

Fig. 5. Representative low-energy structures of gramicidin S $(M+2H)^{2+}$ ions in (a) vacuum and (b) water, obtained by molecular modeling using a dielectric constant of 1.0 and 78, respectively. Intramolecular hydrogen bonding is indicated by dashed lines [79].

The protonated gas-phase biomolecule ions show effects that were observed in model polyfunctional molecules: internal IHBs, multiple IHBs and IHB networks, solvent bridges and competition between internal and external solvation. Some of these features are illustrated in Fig. 5 which also shows that internal IHBs may be displaced by external solvation.

Ionized gas-phase biomolecules generated by electrospray also exhibit new features such as multiple protonation. In fact, this was observed in relatively simple molecules such as diprotonated diamines [77]. The relative PAs of various basic sites on macromolecules, and the effects of partial protonation on the PAs of the remaining basic sites, need to be evaluated as they affect protein conformation and mass spectrometric sequencing. The large and rapidly growing literature on gas-phase biomolecules requires a separate review. This subject constitutes new challenges in gas-phase ion chemistry.

16. Summary

Gas-phase basicites and proton affinites have been measured by various methods over three decades. It now appears that the GB and PA values for a set of reference bases from the main scales are all compatible. This consistency is achieved by anchoring to accurate local standards and by correcting for global, usually $<10\%$ contractions or expansions of the ladders, apparently resulting from temperature effects.

After the adjustments, good agreement is observed among the main sets of data including independent standards from spectroscopic threshold values, relative GB_{600} values from PHPMS and GB_{350} values from ICR, relative PAs from PHPMS temperature studies, and absolute GB and PA values from theory. Some of the assignments in the ladders are also supported independently by kinetic bracketing and by association thermochemistry. An important check is that the entropies of protonation derived from the GB and PA data are structurally reasonable and agree with isoelectronic analogues. This confirms the internal consistency of the data GB and PA data as well as of the entropies of protonation themselves.

Altogether, the consistency of the data from various independent methods suggests that the averaged GB_{298} values in Table 3 and PA values in Table 4 are accurate within $\pm 0.8\,\mathrm{kcal\,mol^{-1}}$ and the S_p values in Table 6 are accurate within $\pm 1.5\,\mathrm{cal\,mol^{-1}\,K^{-1}}$. These average values agree with and further support the tabulated NIST values of Hunter and Lias [1]. This accuracy may represent the limit of current methods and it should be sufficient for most applications.

The gas-phase proton affinities can identify structural effects on the intrinsic molecular basicities. Along with the experimental studies, much effort has been invested in calculating molecular proton affinities and the contributing structural effects. For example, internal hydrogen bonds that can increase the proton affinities of polyfunctional molecules and biomolecules are the subjects of current research.

Importantly, the gas-phase data allow quantifying the solvation thermochemistry of ions and the physical factors that contribute to ion solvation. This analysis reveals that the solvation energies can be assigned to simple molecular factors. In particular, the hydrogen bonding contributions are related in simple additive terms to the number of protic and alkyl hydrogens.

In summary, the last three decades saw a transition in our understanding of acid–base chemistry. Measurements of gas-phase acidities and basicities, their molecular interpretations, and applications to ion clustering and solvation established quantitatively the physical factors that contribute to protonation in the gas phase and in solution. The results transformed organic acid–base chemistry into phenomena that can be interpreted in simple physical terms.

References

[1] E.P. Hunter, S.G. Lias, J. Phys. Chem. Ref. Data 27 (1998) 413;
P.J. Linstrom, W.G. Mallard (Eds.), NIST Chemistry Webbook, NIST Standard Reference Database, NIST, Gaithersburg, MD, 2001.

[2] M. Meot-Ner (Mautner), L.W. Sieck, J. Am. Chem. Soc. 113 (1991) 4448.

[3] J.E. Szulejko, T.B. MacMahon, Int. J. Mass Spectrom. Ion Processes 109 (1991) 279;
J.E. Szulejko, T.B. MacMahon, J. Am. Chem. Soc. 115 (1993) 7839.

[4] B.J. Smith, L. Radom, J. Am. Chem. Soc. 115 (1993) 4885.

[5] A.L.L. East, B.J. Smith, L. Radom, J. Am. Chem. Soc. 119 (1997) 9014.

[6] (a) J.F. Wolf, R.H. Staley, I. Koppel, M. Taagepera, R.T. McIver, J.L. Beauchamp, R.W. Taft, J. Am. Chem. Soc. 99 (1977) 5417;
(b) R.W. Taft, Prog. Phys. Org. Chem. 14 (1983) 248.

[7] R. Yamdagni, P. Kebarle, J. Am. Chem. Soc. 98 (1976) 1320; Y.K. Lau, Ph.D. Thesis, University of Alberta, 1979.

[8] J. Bartmess, in: P.J. Linstrom, W.G. Mallard (Eds.), NIST Chemistry Webbook, NIST Standard Reference Database, NIST, Gaithersburg, MD, 2001.

[9] D.K. Bohme, G.I. Mackay, H.I. Schiff, J. Chem. Phys. 73 (1980) 4976.

[10] M. Meot-Ner (Mautner), F.H. Field, J. Chem. Phys. 66 (1977) 4527.

[11] M.T. Bowers (Ed.), Gas Phase Ion Chemistry, Academic Press, New York, 1979.

[12] D.H. Aue, M.T. Bowers, in: M.T. Bowers (Ed.), Gas Phase Ion Chemistry, vol. 2, Academic Press, New York, 1979, p. 2.

[13] V.L. Talroze, I. Frankevich, Dokl. Acad. Nauk. USSR 111 (1956) 376.

[14] M.J.B. Munson, J. Am. Chem. Soc. 87 (1965) 2332.

[15] J.L. Beauchamp, S.E. Buttrill, J. Chem. Phys. 48 (1968) 1783.

[16] J.I. Brauman, L.K. Blair, J. Am. Chem. Soc. 90 (1968) 5636.

[17] M.T. Bowers, D.H. Aue, H.M. Webb, R.T. McIver, J. Am. Chem. Soc. 93 (1971) 4314.

[18] R.T. McIver, Rev. Sci. Inst. 41 (1970) 555.

[19] F.H. Field, J.L. Franklin, F.W. Lampe, J. Am. Chem. Soc. 79 (1957) 2419;
M.J.B. Munson, F.H. Field, J. Am. Chem. Soc. 88 (1966) 2621.

[20] P. Kebarle, Ann. Rev. Phys. Chem. 28 (1977) 445.

[21] J.J. Solomon, M. Meot-Ner (Mautner), F.H. Field, J. Am. Chem. Soc. 96 (1974) 3727.

[22] S.G. Lias, J.F. Liebman, R.D. Levin, J. Phys. Chem. Ref. Data 13 (1984) 695.

[23] M. Meot-Ner (Mautner), J. Am. Chem. Soc. 104 (1982) 5.

[24] J.W. Keister, J.S. Reiley, T. Baer, J. Am. Chem. Soc. 115 (1993) 12613.

[25] J.C. Traeger, Rapid. Commun. Mass Spectrom. 10 (1996) 119.

[26] L.W. Sieck, J. Phys. Chem. 101 (1997) 8140.

[27] H.M. Rosenstock, R. Buff, M.A.A. Ferreira, S.G. Lias, A.C. Parr, R.L. Stockbauer, J.L. Holmes, J. Am. Chem. Soc. 104 (1982) 2337.

[28] T. Baer, J. Am. Chem. Soc. 102 (1980) 2482.

[29] T. Baer, Y. Song, C.Y. Ng, J.B. Lia, W.W. Chen, J. Phys. Chem. A 100 (1996) 16555.

[30] S.T. Park, S.K. Kim, M.S. Kim, J. Chem. Phys. 114 (2001) 5568.

[31] J.C. Traeger, R.G. McLoughlin, A.J.C. Nicholson, J. Am. Chem. Soc. 104 (1982) 5318.

[32] B. Ruscic, J. Berkowitz, J. Chem. Phys. 101 (1994) 10936.

[33] D.J. Bogan, F.L. Nesbitt, J.L. Stief, J.L. Durant, S.C. Kuo, Z. Zhang, R.B. Klemm, in: Proceedings of the13th International Symposium on Gas Kinetics, University College, Dublin, Ireland, September 11–16, 1995.

[34] J.C. Traeger, J.L. Holmes, J. Phys. Chem. 97 (1993) 3453.

[35] H.F. Prest, W.B. Tzang, J.M. Brom, C.Y. Ng, J. Am. Chem. Soc. 105 (1983) 7531.

[36] E.A. Walters, N.C. Blais, J. Chem. Phys. 80 (1984) 3501.

[37] C.Y. Ng, D.J. Trevor, P.W. Tiedemann, S.T. Ceyer, P.L. Kronebush, B.H. Mahan, Y.T. Lee, J. Chem. Phys. 67 (1977) 4235.

[38] J.A. Pople, L.A. Curtiss, J. Phys. Chem. 91 (1987) 155.

[39] B. Ruscic, J. Berkowitz, L.A. Curtiss, J.A. Pople, J. Chem. Phys. 91 (1989) 114.

[40] J.C. Traeger, Int. J. Mass Spectrom. Ion Processes 66 (1985) 271.

[41] A. Kormornicki, D.A. Dixon, J. Chem. Phys. 97 (1992) 1087.

[42] B. Ruscic, M. Schwaz, J. Berkowitz, J. Chem. Phys. 91 (1989) 6772.

[43] J.C. Traeger, B.M. Kompe, Org. Mass Spectrom. 26 (1991) 209.

[44] M.J. Frisch, H.F. Shaefer III, J.S. Binkley, J. Phys. Chem. 89 (1985) 2192.

[45] M. Meot-Ner (Mautner), L.W. Sieck, Int. J. Mass Spectrom. Ion Processes 109 (1991) 187.
[46] M. Meot-Ner (Mautner), J. Phys. Chem. 95 (1991) 6580.
[47] L.W. Sieck, M. Meot-Ner (Mautner), J. Phys. Chem. 86 (1982) 3646.
[48] M. Meot-Ner (Mautner), P. Hamlet, E.P. Hunter, F.H. Field, J. Am. Chem. Soc. 102 (1980) 6393.
[49] G.S. Gorman, I.J. Amster, Org. Mass Spectrom. 26 (1991) 227.
[50] G. Bouchoux, J.Y. Salpin, D. Leblanc, Int. J. Mass Spectrom. Ion Processes 153 (1996) 37.
[51] G. Bouchoux, J.Y. Salpin, J. Phys. Chem. 100 (1996) 16555.
[52] S.A. McLuckey, D. Cameron, R.G. Cooks, J. Am. Chem. Soc. 103 (1981) 1313.
[53] R.G. Cooks, J.S. Patrick, T. Kotiahao, S.A. McLuckey, Mass Spectrom. Rev. 13 (1995) 287.
[54] R.C. Dunbar, T.B. McMahon, D. Tholmann, D.S. Tonner, D. Slahub, D. Wei, J. Am. Chem. Soc. 117 (1995) 12819.
[55] W.D. Price, P. Schnier, E.R. Williams, J. Phys. Chem. 101 (1997) 664.
[56] S.G. Lias, P. Ausloos, J. Am. Chem. Soc. 100 (1978) 6027.
[57] X. Li, J.A. Stone, Can. J. Chem. 66 (1988) 1288.
[58] K. Hiraoka, P. Kebarle, J. Am. Chem. Soc. 98 (1976) 6119.
[59] K. Hiraoka, P. Kebarle, Can. J. Phys. 53 (1975) 97;
K. Hiraoka, T. Mori, S. Yamabe, Chem. Phys. Lett. 207 (1993) 178.
[60] M. Meot-Ner (Mautner), J. Am. Chem. Soc. 100 (1978) 4694.
[61] M. Meot-Ner (Mautner), M.M. Ross, J.E. Campagna, J. Am. Chem. Soc. 107 (1985) 4825.
[62] K. Norrmann, T.B. McMahon, J. Am. Chem. Soc. 118 (1996) 2449.
[63] M. Meot-Ner (Mautner), S.G. Lias, in: P.J. Linstrom, W.G. Mallard (Eds.), NIST Chemistry Webbook, NIST Standard Reference Database, NIST, Gaithersburg, MD, 2001.
[64] C.A. Deakyne, companion article in this issue.
[65] R. Yamdagni, P. Kebarle, J. Am. Chem. Soc. 95 (1973) 3504.
[66] D. Aue, H.M. Webb, M.T. Bowers, J. Am. Chem. Soc. 95 (1973) 2699.
[67] M. Meot-Ner (Mautner), J. Am. Chem. Soc. 105 (1983) 4906.
[68] R.B. Sharma, A.T. Blades, P. Kebarle, J. Am. Chem. Soc. 106 (1984) 510.
[69] G. Bouchoux, Y. Hoppiliard, R. Houriet, New J. Chem. 11 (1987) 225.
[70] Q.F. Chen, J.A. Stone, J. Phys. Chem. 99 (1995) 1442.
[71] J.E. Szulejko, T.B. McMahon, V. Troude, G. Bouchoux, H.E. Audier, J. Phys. Chem. 102 (1998) 1879.
[72] S. Yamabe, K. Hirao, H. Wasada, J. Phys. Chem. 96 (1992) 10261.
[73] T.R. Furlani, J.F. Garvey, Mol. Phys. 92 (1997) 449.
[74] M. Meot-Ner (Mautner), J. Phys. Chem. 91 (1987) 417.
[75] F. Hillenkamp, M. Karas, R.C. Beavis, B.T. Chait, Anal. Chem. 63 (1991) 1993A.
[76] J.B. Fenn, M. Mann, C.K. Meng, S.F. Wong, Science 246 (1989) 64.
[77] A.T. Blades, J.S. Klassen, P. Kebarle, J. Am. Chem. Soc. 118 (1996) 12437.
[78] M.T. Bowers, P.R. Kemper, G. von Helden, P.A.M. van Koppen, Science 260 (1993) 1446.
[79] D.E. Clemmer, M.F. Jarrold, J. Mass Spectrom. 32 (1997) 577.
[80] D.V. Dearden, Y. Liang, J.B. Nicoli, A.J. Kellersberg, Mass Spectrom. 36 (2001) 989.
[81] S. Campbell, M.T. Rodgers, E.M. Marzluff, J.L. Beauchamp, J. Am. Chem. Soc. 117 (1995) 12840.
[82] M. Meot-Ner (Mautner), J. Am. Chem. Soc. 110 (1988) 3075.
[83] M. Meot-Ner (Mautner), S. Scheiner, W.O. Yu, J. Am. Chem. Soc. 120 (1998) 6980.
[84] C.A. Deakyne, M. Meot-Ner (Mautner), J. Am. Chem. Soc. 121 (1999) 1546.
[85] S.E. Rodriguez-Cruz, J.S. Klassen, E.R. Williams, J. Am. Soc. Mass Spectrom. 8 (1997) 565.
[86] J. Gidden, J.E. Bushnell, M.T. Bowers, J. Am. Chem. Soc. 123 (2001) 5610.
[87] K. Hiraoka, P.J. Kebarle, J. Am. Chem. Soc. 99 (1977) 360.
[88] C.A. Deakyne, M. Meot-Ner (Mautner), C.L. Campbell, S.P. Murphy, J. Chem. Phys. 84 (1986) 4958.